Manuscript 7685 - REV 2

Phase Diagram and Thermal Expansion of orthopyroxene-, clinopyroxene- and ilmenite-structured $MgGeO_3$

Word count: ~7500, excluding captions+tables (~2600 words) and references (~1500 words)

Simon A. Hunt[1, 2, *], James R. Santangeli[2], David P. Dobson[2], Ian G. Wood[2].

1 – Department of Materials, University of Manchester, Sackville Street Building, Manchester. M1 3BB. UK

2 – Department of Earth Sciences, University College London, Gower Street, London. WC1E 6BT. UK

* - simon.hunt@manchester.ac.uk

Abstract

The $MgGeO_3$ system is a low-pressure analogue for the Earth forming $(Mg,Fe)SiO_3$ system and exhibits recoverable orthopyroxene, clinopyroxene and ilmenite structures below 6 GPa. The pressure-temperature conditions of the clinopyroxene to ilmenite phase transition are reasonably consistent between studies, having a positive Clapeyron slope and occurring between 4 and 7 GPa in the temperature range 900-1600 K. There are, though, significant discrepancies in the Clapeyron slope of the orthopyroxene to clinopyroxene phase transition in existing works which also disagree on the stable phase at ambient conditions. The most significant factor in these differences is the method used; high-pressure experiments and thermophysical property

measurements yield apparently contradicting results. Here, we perform both high pressure and temperature experiments as well as thermal expansion measurements to reconcile the measurements. High pressure and temperature experiments, yield a Clapeyron slope of $-1.0^{+1.0}_{-0.7}$ *MPa/K for the* $MgGeO_3$ *orthopyroxene-clinopyroxene phase transition, consistent with previous high pressure and temperature experiments. The* $MgGeO_3$ *orthopyroxene-clinopyroxene-ilmenite triple point is determined to be at 0.98 GPa and 752 K, with the ilmenite phase stable at ambient conditions. The high temperature (> 600 K) thermal expansion of the clinopyroxene phase is greater than that of the other phases. Debye-Grüneisen relationships fitted to the volume-temperature data give Debye temperatures for the orthopyroxene, clinopyroxene and ilmenite phases of 602(7) K, 693(10) K and 758(13) K and* V_0 *of 897.299(16)* $Å^3$*, 433.192(10)* $Å^3$ *and 289.156(6)* $Å^3$ *respectively. The Clapeyron slopes calculated directly from the Debye-Grüneisen relationships are consistent with previous thermophysical property measurements. The presence of significant anharmonicity and/or formation of defects in the clinopyroxene phase at high-temperatures, which is not apparent in the other phases, accounts for the previous contradictions between studies. The inferred increased heat capacity of the clinopyroxene corresponds to an increase in entropy and an expanded phase field at high temperatures.*

Keywords

Equation of State, Heat Capacity, Thermal Expansion, high-pressure, phase transition, anharmonicity

Introduction

The MgO-GeO_2 system has long been studied because of its similarity to the MgO-SiO_2 system but with structure types stable at lower pressures. Like $MgSiO_3$, $MgGeO_3$ transforms from the ilmenite structure to both the perovskite structure (at around 12 GPa, Leinenweber et al. 1994) and the post-perovskite structure (around 65 GPa, Akaogi et al. 2005; Hirose et al. 2005). Below 10 GPa, $MgGeO_3$, like $MgSiO_3$, exhibits orthopyroxene, clinopyroxene and ilmenite structures (Ringwood and Seabrook 1962; Kirfel and Neuhaus 1974; Ozima and Akimoto 1983; Ross and Navrotsky 1988). Both the MgO-GeO_2 and MgO-SiO_2 systems have ambient pressure olivine structures that transform to spinel structures at elevated pressure and temperature (Ross and Navrotsky 1987; Akaogi et al. 1989). The germanate system is not, though, a perfect low-pressure reflection of the silicate system. Pure GeO_2 is stable in the rutile structure at ambient conditions and above 1310 K transforms to that of quartz (Laubengayer and Morton 1932). This contrasts with SiO_2, in which quartz is the ambient pressure phase and the rutile structure is stable above 9 GPa as stishovite. These two silica phases are separated by coesite, which has not been found in GeO_2. Neither has the wadsleyite (β-Mg_2SiO_4) structure been observed in Mg_2GeO_4. Above about 4 GPa and 1000 K in $MgGeO_3$, the ilmenite structure is stable and there is no appearance of the $Mg_2SiO_4 + SiO_2$ field that separates the clinopyroxene and ilmenite phases in the $MgSiO_3$ system. An additional intermediate phase occurs in the MgO-GeO_2 binary that is not present in the MgO-SiO_2 binary. Initially reported as Mg_4GeO_6 (Robbins and Levin 1959; McCormick 1964) and subsequently refined to be $Mg_{3.5}Ge_{1.25}O_6$ with space group *Pbam* (von Dreele et al. 1970; Kostiner and Bless 1971), at ambient pressure it is stable below 1768 K, whereupon it breaks down to $Mg_2GeO_4 + MgO$ (Robbins and Levin 1959).

There is more reported complexity in the silicate pyroxenes (e.g. Ohi and Miyake 2016) than in the germanate equivalents. Silicate clinopyroxene, with the space group *C*2/*c*, is stable above about 7 GPa (Ulmer and Stalder 2001). At low pressures, this transforms to either low-clinoenstatite (space group $P2_1/c$) or, above 1073 K, orthoenstatite (space group *Pbca*). Above ~1270 K, orthoenstatite transforms to an unrecoverable protoenstatite (space group *Pbcn*) (Murakami et al. 1982).

Only the orthoenstatite (*Pbca*) and high-clinopyroxene (*C*2/*c*) structures have been recovered in $MgGeO_3$, although the low-clinopyroxene form has been observed in other pyroxene-structured germanates (e.g. $LiFeGe_2O_6$, Redhammer et al. 2010). At ambient pressure, Robbins and Levin (1959) report that orthopyroxene-$MgGeO_3$ transforms to a high-clinopyroxene structure (*C*2/*c*) above 1828±5 K. They comment that it is possible that the high-clinopyroxene phase is the back-transformation product of a 'proto-pyroxene' phase. This would be consistent with the $MgSiO_3$-$MgGeO_3$ binary that has the enstatite—protoenstatite transition temperature increasing from ~1310 K to 1620 K between 0 and 12.5 mol.% $MgGeO_3$ (Sarver and Hummel 1963). In addition, Lyon (1968) compared the observed diffraction peaks of the recovered high-temperature clinopyroxene phase unfavourably to the *C*2/*c* space group but did not make or analyse the clinopyroxene himself. Ozima and Akimoto (1983) argued that protoenstatite is the stable $MgGeO_3$ phase above ~1200 K but this is in disagreement with most other studies.

At pressures greater than ~4 GPa $MgGeO_3$ adopts the ilmenite structure (Kirfel and Neuhaus 1974; Ozima and Akimoto 1983; Ross and Navrotsky 1988) (Figure 1). The clinopyroxene-ilmenite phase boundary is at lower pressure in the study of Ross and Navrotsky (1988) but is conceivably within the systematic errors of the experiments.

Insert Figure 1 here.

There however remains disagreement between studies as to the phase diagram of $MgGeO_3$ below the ilmenite stability field. The extensive experimental study of Kirfel and Neuhaus (1974) proposed a negative Clapeyron slope for the orthopyroxene-clinopyroxene phase boundary with orthopyroxene as the low-temperature–low-pressure phase (Figure 1a). This is topologically consistent with Ringwood and Seabrook (1962) who, though, synthesised the clinopyroxene phase at 0.5 GPa. They therefore questioned whether the shallowness of the phase boundary was caused by shear stresses rather than pressure, as has been observed in natural pyroxenes (Coe and Kirby 1975). Yamanaka et al. (1985) transformed pre-synthesised clinopyroxene phase to orthopyroxene phase at ~1173 K and ambient pressure and attempted, but did not observe, the reverse orthopyroxene to clinopyroxene phase reaction at 973 K and ambient pressure. The phase boundaries of Kirfel and Neuhaus (1974) are consistent with the high-pressure and temperature experimental constraints of Ross and Navrotsky (1988) (Figure 1b) but not with the positive Clapeyron slope derived by calorimetric measurements. The calorimetric Clapeyron slope makes the clinopyroxene phase the low-temperature–low-pressure phase and the stable phase at ambient conditions. Interestingly, the reported experimental results of both Kirfel and Neuhaus (1974) and Ross and Navrotsky (1988) are consistent with the reported sample synthesis conditions of all other studies (Roth 1955; Ringwood and Seabrook 1962; Liebermann 1974; Sato et al. 1977; Kirfel et al. 1978; Ito and Matsui 1979; Ashida et al. 1985; Okada et al. 2008) (Figure 1b) except that of Ozima and Akimoto (1983) (Figure 1c).

Ozima and Akimoto (1983) grew orthopyroxene phase and two types of clinopyroxene $MgGeO_3$ crystals from flux at ambient pressure. They argued that clinopyroxene is the low temperature phase, which transforms to ortho- and the proto-pyroxene structures with increasing

112 temperature. They also reported the stability of orthopyroxene phase between 3 and 5 GPa and
113 ~1300 K where all other authors report the clinopyroxene phase.

114 Only a few measurements of the thermophysical properties of $MgGeO_3$ phases have been
115 made. Ross and Navrotsky (1988) used high temperature solution calorimetry and room
116 temperature vibrational spectroscopy measurements of the three phases which they amalgamated
117 to produce a thermodynamically consistent phase diagram (Figure 1b). Yamanaka et al. (1985)
118 measured the thermal expansion and thermal evolution of the crystal structures of the ortho- and
119 clinopyroxene phases between 293 K and 1373 K, but only with very large temperature steps.
120 Ashida et al. (1985) measured the room-temperature compressibility, thermal expansion between
121 300 and 1000 K, and heat capacity of ilmenite-structured $MgGeO_3$ between 150 and 700 K.
122 Tsuchiya and Tsuchiya (2007) used density functional theory to compute an thermal equation of
123 state for ilmenite-structured $MgGeO_3$ but did not investigate the pyroxene phases.

124 In this study, we attempt to unify the differing phase diagram topographies presented by
125 experiments and thermodynamics. We performed high pressure and temperature quenching
126 experiments to directly constrain the phase diagram of the $MgGeO_3$ system and we also measured
127 the thermal expansion of the three phases at ambient pressure. Fitting the thermal expansion
128 volumes with a Debye-Grüneisen zero-pressure equation of state enables us to estimate the heat
129 capacity and Clapeyron slope of the phase relations to compare with the direct experimental
130 constraints.

131

132

133

134

Methods

Sample Synthesis and high-pressure Phase Relations

Samples of orthopyroxene-structured $MgGeO_3$ were synthesised from stoichiometric mixtures of MgO and GeO_2. The oxides were ground in an agate pestle and mortar under isopropanol and pressed into pellets. The pellets were sintered at 1373 K for 72 h in air. Pellets were then crushed and ground under isopropanol for 20 minutes to generate a fine powder and analysed by X-Ray powder diffraction to determine their purity. This sintering and analysis process was repeated, with minor additions of MgO or GeO_2 based on the phase fractions determined from the diffraction patterns, until pure orthopyroxene-structured $MgGeO_3$ was synthesised.

Phase relations of $MgGeO_3$ at pressures less than ~1.5 GPa were examined using a piston-cylinder cell (Boyd and England 1960) and above ~1.5 GPa with a Walker type multi-anvil apparatus (Walker et al. 1990) at University College London. Multiple samples ($MgGeO_3$ and pressure calibrants) were contained in capsules of double wrapped 25 μm Inconel625 ($Ni_{61}Cr_{22}Mo_9Fe_5$) foil, 3 mm long and 2.5 mm diameter; the samples were separated by disks of Inconel625.

Piston-cylinder experiments used $BaCO_3$ pressure media with graphite furnaces (OD 7.7 mm, ID 6.2 mm) and the inner parts of the cell, surrounding the capsule, were made from MgO. The capsule was loaded centrally with respect to the length of the furnace. Temperature was monitored using a K-Type thermocouple which was 1 mm above the end of the sample capsule (2.5 mm above the centre of the furnace). A 1 mm thick corundum plate was placed between the sample capsule and the end of the thermocouple to prevent sample deformation.

The multi-anvil assembly used an 18 mm octahedral cell compressed by anvils with 11 mm corner truncations. The furnace comprised a 14 mm long double wrap of 25 μm thick Inconel 625

158 foil, with a diameter of 4 mm, inside a zirconia sleeve with an outer diameter of 6.25 mm. The
159 inner parts were made of MgO as a confining medium and were large enough to hold the 3 mm
160 long by 2.5 mm in diameter capsule. Temperature was monitored at the end of the sample capsule
161 using a D-type ($W_{97}Re_3$—$W_{75}Re_{25}$) thermocouple. Thermocouples were shielded from the furnace
162 using thin walled corundum tubes with 0.8 mm outer diameter. The effects of pressure on
163 thermocouple-emf were assumed to be negligible. The multi-anvil cell was calibrated using SiO_2,
164 Ni_2SiO_4, Fe_2SiO_4 and Mg_2GeO_4 phase relations, in the same experiments as the $MgGeO_3$ phase
165 relations were determined. The pressure calibrations indicated a large decrease in pressure in the
166 temperature range 870-1370 K. The average pressure depression was 1.9 GPa, relative to a Bi
167 calibration curve measured at room temperature.

168 The conditions of the synthesis and phase relations experiments, as well as the run products
169 are listed in Table 1. The phases in all recovered samples were identified by X-ray diffraction. The
170 phase boundary positions were determined by the first occurrence of the high pressure phase and
171 pass thought the middle of the constraints. The experiments that constrain the position of the phase
172 boundaries are noted in Table 1.

173 The samples of the high-pressure clinopyroxene-structured and ilmenite-structured
174 $MgGeO_3$ for thermal expansion measurements were synthesised from the orthopyroxene phase
175 using the same 18/11 multi-anvil cell. The clinopyroxene-structured $MgGeO_3$ was synthesised at
176 2.5 GPa and 1173 K for 3 hours and $MgGeO_3$ ilmenite phase was synthesised at 5 GPa and 1373
177 K for 3 hours. Each sample synthesis was recovered, ground in an agate pestle and mortar under
178 isopropanol before analysis by X-ray powder diffraction to confirm phase purity. Several syntheses
179 were required to produce the amount of material required for the thermal expansion measurements.

180 **Thermal Expansion Measurements by X-ray Powder Diffraction**

Ideally, all three samples would be measured by X-ray diffraction simultaneously, removing the possibility of any inconsistencies between measurements. However, there is a significant degree of peak overlap between the orthopyroxene phase and the other phases due to the large number of diffraction peaks in the orthopyroxene phase (see Figure 2). The orthopyroxene phase was therefore run on its own while the clinopyroxene and ilmenite phases were mixed together and measured at the same time. The samples used for the diffraction experiments were mixed with high purity MgO (Aldrich 99.99%). The MgO was fired overnight at 1073 K in air before mixing. The purpose of the MgO was to provide good constraints to the specimen transparency and displacement in the subsequent refinements – constraints that are not well provided by low symmetry materials.

Insert Figure 2 here.

Unit-cell volumes as a function of temperature were investigated by X-ray diffraction using the same method as previous studies (e.g. Hunt et al. 2017; Pamato et al. 2018). We used a PANalytical X'Pert Pro diffractometer, with Bragg–Brentano parafocusing reflection geometry. The cobalt X-ray source is monochromated, by a Ge (1 1 1) Johansson geometry focusing monochromator, to produce a Co $K\alpha_1$ incident beam, the wavelength of which is assumed to be 1.788996 Å (Hölzer et al. 1997). The X-ray tube was operated at 40 kV and 30 mA. Variable-width divergence and anti-scatter slits were used, together with a 10 mm wide incident-beam mask, so as to illuminate a 10 × 8.5 mm area of the sample. Both the incident and diffracted beams had 0.04 radian Soller slits to reduce the axial divergences. The X-ray detector was an 'X'Celerator' position-sensitive detector with an angular range of $2\theta = \pm 1.061°$ and an effective fixed step size

of 0.0167°. Data were collected over the 2θ range from 20° to 154.9°. Prior to the experiments reported here, the zero 2θ angle of the diffractometer was determined using an Si standard.

Diffraction data between 40 and 300 K were collected using an Oxford Cryosystems PheniX-FL low-temperature stage (Wood et al. 2018) and between 298 and 1173 K using an Anton Paar HTK1200N heated stage. The data were collected starting with the lowest temperature, in 20 K steps for the low-temperature stage and in 25 K steps for the high-temperature stage. In the PheniX-FL cold stage, the sample was held in an atmosphere of helium exchange gas. The temperature was cooled as quickly as possible (~3 K min^{-1}) to 80 K and then at 1 K min^{-1} to 40 K. After equilibration for 10 min at 40 K the data were collected. Subsequent increases in temperature were at 1 K min^{-1} and the data were measured after approximately 15 min equilibration. The data collections were ~90 min long. In the high-temperature stage, the sample was heated at 5 K min^{-1}, after which it was equilibrated for 10 min and the data collected in a time of ~90 min.

Measurements in the high-temperature stage were made with the sample chamber open to the atmosphere. Data were collected in the orthopyroxene phase up to 1173 K. No additional diffraction peaks, produced by either back-transformation of the high pressure phases to orthopyroxene-$MgGeO_3$ or by reaction to form olivine-Mg_2GeO_4, were observed in any of the high temperature measurements or in diffraction patterns taken from the samples after recovery to room temperature. The measurements of the clinopyroxene and ilmenite phases were stopped at 923 K when an additional diffraction peak appeared in the data.

The data were analysed using the GSAS suite of programs (Larson and Von Dreele 2000; Toby 2001), after conversion from variable to fixed divergence slit geometry by the diffractometer

226 manufacturer's X'pert HighScorePlus software package. The data was refined sequentially starting
227 at with the data collected closest to room temperature. The initial model for each refinement was
228 the converged fit of the preceding temperature, except for the data closest to room temperature
229 which used the volumes and atomic coordinates from Yamanaka et al. (1985, 2005) as their starting
230 point. Example diffraction patterns, from orthopyroxene and clinopyroxene + ilmenite, collected
231 at 298 K are presented in Figure 2.

232 As has been previously found, the diffraction patterns of the clinopyroxene phase showed
233 all the peaks consistent with the space group $C2/c$ and none of the additional peaks indicative of
234 the $P2_1/c$ space group. The clinopyroxene (space group $C2/c$) and ilmenite (space group $R\bar{3}$)
235 phases were analysed using the Le Bail method (Le Bail et al. 1988). The Le Bail method produces
236 less biased cell parameters when fitting data from samples that might not be a true random powder
237 pattern but at the cost of freely adjusting the intensity of each sample peak. In each refinement, the
238 lattice parameters for the two $MgGeO_3$ phases (the triple-hexagonal cell was used for the ilmenite)
239 and MgO (space group $Fm\bar{3}m$) were refined. Also refined were the peak profiles, specimen
240 displacement and transparency, which were constrained to be the same for each sample in the
241 diffraction pattern. At each temperature the fit achieved convergence with the data.

242 The larger unit-cell and many overlapping low-intensity peaks in the orthopyroxene phase
243 (space group *Pbca*) prevent the Le Bail method from producing well constrained fits to the
244 diffraction data. Therefore the Rietveld method of refinement was used (Rietveld 1969). All the
245 atoms in each phase (orthopyroxene-structured $MgGeO_3$ or MgO) were constrained to have the
246 same isotropic thermal parameters (Uiso) and the two phases were constrained to have the same
247 specimen transparency and displacement. Each pattern in the temperature series was initially fitted
248 for the background coefficients and the unit cells of the MgO and orthopyroxene-structured

249 $MgGeO_3$ phases, whilst the peak profile parameters, atomic positions and thermal parameters of
250 the orthopyroxene phase were fixed. When this refinement had converged these parameters were
251 sequentially allowed to refine until all parameters were determined.

252 In the initial fits of the orthopyroxene phase data there was a correlation between the unit-
253 cell parameters and the poorly constrained sample transparency. Therefore, the data were re-fitted
254 with a fixed sample transparency. For the low-temperature stage data, the mean of the consistent
255 transparencies was used. For the high-temperature stage data, the free-fit transparencies decreased
256 with temperature, slowly below 773 K and more quickly at higher temperatures. These values were
257 smoothed using two 1st degree polynomials which intersected at the change in slope in the
258 transparency values. The data were subsequently re-refined using the transparency value of the
259 polynomial at the relevant temperature.

260 In both 40 K diffraction patterns, reflections from β-nitrogen were observed. It was
261 included in the refinement with space group $P6_3/mmc$. Following the unphysical model of Vegard
262 (1932), the N_2 molecules were assumed to be spherical and the size compensated for by unusually
263 large thermal vibrations.

264 There is a small offset (<2 in 10^4) in the lattice parameters and volumes between the high
265 and low temperature diffraction stages. To compensate for this in the subsequent analysis the high
266 temperature data were multiplied by a scale factor to align them with the low temperature data.
267 The scaling was done by minimising the residuals of a third-degree polynomial passing through
268 the 10 data between 220–398 K. The scaling factors are listed in Table 3. The scaling has minimal
269 effect on the fitted thermophysical parameters; with and without scaling the data, they were all
270 within two standard errors of each other and most parameters were within one standard error.
271

Results

Phase Relations at high pressure and temperature

The pressure-temperature conditions at which we have synthesised the different phases of $MgGeO_3$ are presented in Figure 3a and Table 1. The phase boundaries constrained here are compared to those of other studies in

Figure 3b. We find that below ~ 900 K the reaction kinetics are slow and the reaction does not run to completion even after 20 hrs. This is consistent with the inferred experimental constraints of Kirfel and Neuhaus (1974) who report no experiments below 923 K. Above ~ 900 K reaction kinetics are fast, running to completion within 1 hour at 1123 K and 24 hours at 973 K.

Insert Figure 3 here.

Insert Table 1 here.

There is disagreement between studies as to which phase is the stable phase of $MgGeO_3$ between ~ 900 K and 1273 K at ambient pressure (Figure 1). Kirfel and Neuhaus (1974) find the orthopyroxene phase is stable in this temperature range (Figure 1a), whilst Ross and Navrotsky (1988) argue the clinopyroxene phase is the stable ambient pressure below 973 K (Figure 1b). Ozima and Akimoto (1985) argue the orthopyroxene phase is stable between 1083 and 1173 K, transforming to the clinopyroxene or protopyroxene phase at lower and higher temperatures respectively.

During our high-temperature stage X-ray diffraction measurements (up to 1173 K) we did not observe any sign of the orthopyroxene phase transforming to the clinopyroxene phase despite the sample being hotter than 900 K for over 34 hours and hotter than 1023 K for 22 hours by the end of the experiment. However, during the clinopyroxene and ilmenite phase X-ray diffraction measurements, a new diffraction peak appeared around 900 K; identification of which was prevented by termination of the measurement. No phase transformation is to be expected at temperatures less than 900 K based on the reaction kinetics inferred from the high -pressure experiments in this study. Therefore, the onset of reaction around 900 K in the clinopyroxene or ilmenite phase but not in the orthopyroxene phase indicates that the orthopyroxene phase is the stable phase at ~ 900 K and ambient pressure. Between 900 K and 1173 K, the orthopyroxene phase remains the stable phase on the basis that there is no sign of transformation during the X-ray diffraction measurements. This is consistent with the observations of Yamanaka et al (1985), who transformed the clinopyroxene phase to orthopyroxene at 1173 K in 1 hour but the orthopyroxene phase showed no signs of transformation after 24 hours at 973 K. The orthopyroxene phase is therefore shown to be the stable phase at ambient pressure at temperatures between 900 K and 1828±5 K. We note that it is not possible to determine if the orthopyroxene phase ceases to be the stable phase below 900 K because of retarded reaction kinetics.

Our experimental phase diagram is consistent with most of the previous experimental data (Figure 1) and like previous studies we find that ilmenite-structured $MgGeO_3$ is the high pressure phase. The clinopyroxene—ilmenite phase boundary is constrained to have a Clapeyron slope of 6.4 + 0.1/-0.6 MPa/K and to intercept 0 GPa at 600 K. This is in better agreement with the experimentally constrained 5.45 MPa/K of Kirfel and Neuhaus (1974) (Table 2) than the value of 1.9(4) MPa/K calculated by Ross and Navrotsky (1988) from calorimetry data. Our

clinopyroxene—ilmenite phase boundary is ~ 1GPa lower in pressure than that of Kirfel and Neuhaus (1974) (Figures 1a, 3b) which could be due to differences in pressure calibration between the studies.

Insert Table 2 here.

The orthopyroxene-clinopyroxene phase boundary occurs at <1 GPa, consistent with the experiments of Ringwood and Seabrook (1962) and Kirfel and Neuhaus (1974). Our experiments give a Clapeyron slope of -1.0 +1.0/-0.7 MPa/K which intercepts 0 GPa at 1736 K. Given that the phase boundary is sub-parallel to the temperature axis, the value of 1736 K is very close to the 1 atmosphere value of 1828 K determined by Robbins and Levin (1959). Our phase boundary is in excellent agreement with the study of Kirfel and Neuhaus (1974); who also have a negative but slightly shallower Clapeyron slope of -0.82 MPa/K but who fixed their 0 GPa intercept to be 1828 K (Table 2, Figures 1 and 3). Our phase boundary would be in even better agreement with Kirfel and Neuhaus (1974) if we also fixed the 0 GPa intercept to 1828 K. These results contradict the studies of Ozima and Akimoto (1983) and Ross and Navrotsky (1988) who both argued for a positive Clapeyron slope.

Ozima and Akimoto (1983) report simultaneously flux growing orthopyroxene, clinopyroxene and 'clinopyroxene from protopyroxene' phases in the temperature range 928-1228 K. Yamanaka et al. (1985) quenched the orthopyroxene phase from a flux at 1823 K and recovered the clinopyroxene phase by slow cooling from a flux at 1633 K. Both studies argue for *C*2/*c* clinopyroxene as the low temperature phase and neither report observing a $P2_1/c$ low-clinoenstatite phase. Ozima and Akimoto (1983) argue for the protoenstatite phase being stable

above 1173 K based on the recovery of two different styles of clinopyroxene phase from their flux. The incompatibility of these studies with our and other studies is possibly due to flux contamination compared to direct growth from oxides.

The phase boundaries in our experiments converge towards lower pressure and temperature and in the absence of other phases the triple point is at 0.98 GPa and 752 K. This is in good agreement with the triple point position of Kirfel and Neuhaus (1974) which is at 1.07 GPa and 517 K.

Thermal Expansion

The unit-cell volumes of the $MgGeO_3$ orthopyroxene, clinopyroxene and ilmenite phases are listed in Table 3 and plotted, as normalised values, in Figures 4, 5 and 6 respectively. The unit-cell parameters measured here at 298 and 300 K show a good correspondence to previously reported values at ambient conditions (Table 4) and have significantly lower standard errors. Our values for clino- and orthopyroxene phases are within the range of previous values. For the ilmenite phase our more precise values correspond reasonably to those of previous studies; our measured unit-cell volume and *c*-axis agree within 2 standard errors and the *a*-axis agrees to 5 standard errors of the values of Ashida et al (1985).

Insert Table 3 here.

Insert Figure 4 here.

Insert Figure 5 here.

Insert Figure 6 here.

Insert Table 4 here.

Only two other studies have reported high-temperature unit-cell parameters for the $MgGeO_3$ phases studied here: Yamanaka et al. (1985) and Ashida et al. (1985). Yamanaka et al. (1985) report the unit-cell parameters of clinopyroxene-structured $MgGeO_3$ at five temperatures between 298 and 1023 K and at 298, 1223 and 1373 K for the orthopyroxene-structured $MgGeO_3$. Their unit cell parameters are always larger than those reported here (Figure 4 and Figure 5) and the difference between their data and ours increases with temperature. Conversely, the unit-cell volumes from Ashida et al. (1985) are always smaller than those measured here; again the difference increases with temperature. The increasing differences in unit cell parameter with temperature might imply that the differences come from inaccuracies in thermometry. We have calibrated our experimental apparatus using the melting point of gold (Pamato et al. 2018) and the thermal expansivity of silicon (Lindsay-Scott et al. 2007) and find excellent agreement with literature data for these two calibration methods. We therefore believe the present thermometry and unit-cell parameter measurements to be the most accurate of the three studies. If the differences between the present data and the previous studies are due to inaccuracies in thermometry it would require temperature errors in excess of 10% in the previous studies.

374 The Le Bail method does not give the atomic positions of the atoms within the unit-cell but
375 the Rietveld refinement used for the orthopyroxene phase gives atomic positions which, while
376 poorly constrained, are overall consistent with those of Yamanaka et al. (1985).
377
378 **Volume-temperature models.** For many materials, at elevated temperatures (>298 K), the change
379 in unit-cell volume and axes with temperature is well approximated by the integral over a low
380 degree polynomial. This empirical form of thermal expansion has the formulation (Fei 1995):

$$l(T) = l_{T_{\mathrm{ref}}} \exp\left[\int_{T_{\mathrm{ref}}}^{T} \alpha\,(T)\mathrm{d}T\right] \qquad 1$$

381 where $l_{T_{\mathrm{ref}}}$ is a unit-cell parameter (i.e. V, a, b, c) at a reference temperature, T_{ref}, and $\alpha(T)$ is the
382 thermal expansivity, the 2nd degree form of which is:

$$\alpha(T) = a_0 + a_1 T + a_2 T^{-2} \qquad 2$$

383 Here, the reference temperature is taken as 298 K and values of $l_{T_{\mathrm{ref}}}$, a_0, a_1 and a_2 for the unscaled
384 high-temperature stage data in this study are listed in Table 5. Also listed are the equivalent
385 parameters for the experimental data of Yamanaka et al. (1985) and Ashida et al. (1985) as well
386 as calculations of Tsuchiya and Tsuchiya (2007). The data density of this study enabled utilisation
387 of the 2nd degree form of the thermal expansivity but the more sparse data of the other studies mean
388 it is only reasonable to report the 0th or 1st degree forms.
389

Insert Table 5 here.

390
391 For the clinopyroxene phase, except for the β angle, the values of a_0 derived from the study
392 of Yamanaka et al. (1985) are more than one standard error greater than those in this study, which

393 is not unexpected given their larger unit-cell parameters. Only the volumetric thermal expansivity
394 of the ilmenite-structured phase is calculable from the data of Ashida et al. (1985) and this is within
395 error of our value at the reference temperature (298 K) but does not increase at the same rate as
396 that of this study. Again this might be expected because of the smaller volumes measured in that
397 study.

398 In the orthopyroxene phase, the axial thermal expansions occur in the same order as those
399 of Yamanaka et al. (1985), $\alpha_b > \alpha_c > \alpha_a$, but with slightly different values. In the clinopyroxene
400 phase both studies agree that $\alpha_b > \alpha_a > \alpha_c$. The order of these axial thermal expansions is the same
401 as those in the equivalent polymorphs in $MgSiO_3$ (Hugh-Jones 1997).

402 For the ilmenite phase, the calculated thermal expansion of Tsuchiya and Tsuchiya (2007)
403 is less than that measured here.

404

405 At low-temperatures the thermal expansion does not follow a simple low-order polynomial form.
406 Instead, the Debye model can be used to provide a theoretical description of the internal energy
407 (U) that, when combined with further theory, leads to a representation of the thermal expansion
408 that has the observed low-temperature functional form. The internal energy predicted by the Debye
409 model is (e.g. Poirier 2000):

$$U(T) = 9Nk_{\mathrm{B}}T\left(\frac{T}{\theta_{\mathrm{D}}}\right)^3 \int_0^{\theta_{\mathrm{D}}/T} \frac{x^3}{\exp(x)-1}\,\mathrm{d}x \qquad 3$$

410 where N is the number of atoms in the unit cell, k_B is Boltzmann's constant and θ_D is the Debye
411 temperature. The purely harmonic oscillators in this model do not predict thermal expansion and,
412 therefore, this model has been combined with the Grüneisen approximations to form a zero
413 pressure, quasi-harmonic, equation of state (Wallace 1998), in which the effects of thermal

414 expansion are considered equivalent to elastic strain, induced by thermal pressure. Further
415 expansions to the internal energy model that account for intrinsic anharmonicity (Oganov and
416 Dorogokupets 2004) have also been developed. Previous studies (e.g. Vočadlo et al. 2002;
417 Lindsay-Scott et al. 2007) have shown that a second order Grüneisen approximation, combined
418 with quasi-harmonic Debye internal energy model, provides a satisfactory description of data
419 covering a wide range of temperatures, albeit sometimes additional modifications are required (e.g.
420 Hunt et al. 2017; Pamato et al. 2018). It has the form (Wallace 1998):

$$V(T) = V_0 + \frac{V_0 U}{Q - bU} \quad (4)$$

421 where

$$Q = V_0 K_0 / \gamma \quad (5)$$

422 and

$$b = (K' - 1)/2 \quad (6)$$

423 $V(T)$ is the unit-cell volume at finite temperature, V_0 is its 0 K value, K_0 and K' are the bulk modulus
424 and its first pressure derivative, and γ is a Grüneisen parameter, which in the derivation is assumed
425 to be constant. In assuming that γ is independent of temperature it becomes equivalent to the
426 thermodynamic Grüneisen parameter, γ_{th} (Wallace 1998); for a full explanation the reader is
427 referred to Poirier (2000) and Wallace (1998). Expressions of the same functional form as Equation
428 4 may also be used to describe the behaviour of the axes of the crystal but with different
429 interpretation of the values of the parameters Q and b (Lindsay-Scott et al. 2007).

430 Equation 4 was fitted to the unit-cell parameter—temperature data by minimising the sum
431 of the weighted least-squared residuals; the axial values were fitted as measured, rather than
432 pseudo-cubic values. The standard errors of the measurements were used to calculate the weights.
433 Unlike in our previous studies (Hunt et al. 2017; Pamato et al. 2018) the 40 K data point was not

434 additionally weighted because of greater scatter in the low-temperature unit-cell parameters of the
435 orthopyroxene phase. The additional scatter is possibly due to the increased number peaks in the
436 orthopyroxene unit-cell and the larger numbers of free parameters in the GSAS fitting. We expect
437 this scatter to have only a minor effect on the subsequent analysis.

438 There is a suggestion of negative thermal expansion in orthopyroxene phase at the lowest
439 temperatures, both in the axial and volumetric values. The 40 K data, where the negative thermal
440 expansion may be observed, is also where we observe β-N_2 in the diffraction pattern. The data
441 density and 40 K temperature limit of the PheniX-FL stage preclude fitting the data with multiple
442 Debye or Einstein internal energy modes. We note that negative thermal expansion is observed at
443 low temperatures in the germanate pyroxenes $CoGeO_3$ (Redhammer et al. 2010a) and $P2_1/c$
444 $LiFeGe_2O_6$ (Redhammer et al. 2010b) but not in the silicate jadeite (Knight and Price 2008).

445 Table 6 lists the thermophysical parameters returned by the fit and the values derived from
446 these. The fits are plotted in Figures 4, 5 and 6 as lines. The model provides a good fit to the data,
447 except at perhaps the very lowest temperatures in the orthopyroxene phase. The residuals are
448 slightly systematic with temperature but higher and lower order Grüneisen approximations result
449 in worse fits. There is not sufficient temperature range in the data to adequately constrain
450 anharmonic internal energy models (Oganov and Dorogokupets 2004).

451 For each phase, the volumetric Debye temperature is bracketed by the axial Debye
452 temperatures and, for each phase, the a_0 values (Equation 2, Table 5) are proportional to $1/Q$ (Table
453 6). The Debye temperatures reported from heat capacity by Ashida et al. (1985) for ilmenite phase
454 (Table 6) are larger than we calculate here, whereas the Debye temperatures calculated for
455 clinopyroxene and ilmenite phases from the sound velocity data of Liebermann (1974) are slightly
456 smaller. The acoustic Debye temperature has been found to be up to ~80 K lower than the thermal

Debye temperature in pyroxene structured phases (Yang and Ghose 1994) and it would appear that same is true for ilmenite structured phases.

Insert Table 6 here.

The values of *b* imply volumetric K′ values (Table 6) significantly greater than the 3.6 measured in ilmenite-structured $MgGeO_3$ (Ashida et al. 1985) and the 4.59 calculated for ilmenite-structured $MgGeO_3$ (Tsuchiya and Tsuchiya 2007). They are also greater than the values of K′ typically reported for oxides and silicate minerals ($3 < K' < 8$, Knittle 1995). The values of K′ in $MgSiO_3$ pyroxenes have been measured to be greater than 5.6(29) (Angel and Hugh-Jones 1994; Angel and Jackson 2002) but no values exist for $MgGeO_3$ pyroxene-structured phases.

The Grüneisen parameter (γ, Equation 5) is derived using the bulk modulus. The bulk modulus of ilmenite-structured $MgGeO_3$ has been measured to be 187(2) GPa (Sato et al. 1977), 195 GPa (Ashida et al. 1985) and 180(2) GPa (Yamanaka et al. 1985). The bulk modulus of orthopyroxene-structured $MgGeO_3$ is 115 GPa (Kandelin et al. 1983, Ross and Navrotsky 1988) and Liebermann (1974) measured K_s = 131 GPa at 0.75 GPa pressure in the clinopyroxene phase. The adiabatic bulk modulus (K_s) is related to the isothermal Bulk modulus (K_T) by:

$$K_S = K_T(1 + \gamma_{th}\alpha T) \qquad 7$$

Assuming that K_T is isothermal and equal to K_0 and that γ_{th}, the thermodynamic Grüneisen parameter is equal to γ (Equation 5, Wallace 1998), it is possible to solve for γ using a value of K_S.

Using the values above and for the clinopyroxene phase Equation 7, we calculate γ to be 0.86, 1.01 (at 300 K) and 1.23 for the orthopyroxene, clinopyroxene and ilmenite phases respectively (Table 6). The effect of converting K_s to K_T for the clinopyroxene phase is minimal;

calculating γ directly using K_S yields a value of 1.02(1). For ilmenite, Tsuchiya and Tsuchiya (2007) used density functional theory to calculate a value for γ of 1.24, which is very close to our value.

The thermal expansivity (α) is the derivative of the unit-cell parameter with respect to temperature:

$$\alpha(T) = \frac{1}{l(T)}\left(\frac{\mathrm{d}l}{\mathrm{d}T}\right) \quad (8)$$

where l is the unit cell length (for axial expansivities) or volume (for volumetric expansivities). The point-to-point volumetric thermal expansivity of the $MgGeO_3$ phases is plotted in Figure 7, together with the thermal expansion calculated from the polynomial and Debye-Grüneisen models. At low temperatures the orthopyroxene phase has a greater thermal expansion than the clinopyroxene or the ilmenite phases, which is reflected in the lower Debye temperature in this phase (Table 6). Consistent with the polynomial thermal expansion coefficients and the *b*-values of the Debye model, at elevated temperatures, the thermal expansivity of the orthopyroxene phase increases with temperature significantly slower than that of the other two phases.

Insert Figure 7 here.

Heat Capacity

The Debye model of internal energy also can be used to calculate a heat capacity. The isochoric or volumetric heat capacity is the change in internal energy (U), at constant volume, with temperature:

$$C_V = \left(\frac{\partial U}{\partial T}\right)_V \quad (9)$$

The molar heat capacity derived from the Debye model for internal energy (Equation 3) is therefore:

$$C_V = 9nN_A k_B \left(\frac{T}{\theta_D}\right)^3 \int_0^{\theta_D/T} \frac{x^4}{(exp(x)-1)^2} dx \quad (10)$$

where n is the number of atoms per formula unit and N_A is Avogadro's number. Equation 10 uses Debye theory and so at high-temperatures asymptotes to the classical limit $3Nk_B$, known as the Dulong-Petit law. The volumetric heat capacity (Equation 10) can be obtained using the Debye temperatures calculated in the fit to the thermal expansion from Equations 4 and 7.

Whilst this can sometimes be preferred, this limit does not take into account factors such as anharmonicity, or disordering (including defect formation), which are important because they can raise the heat capacity of a material beyond the classical limit. Therefore, an alternative formulation of the heat capacity is to use the coefficient of thermal expansion, the thermodynamic Grüneisen parameter (γ_{th}) and the incompressibility (K) to calculate C_V as (Poirier 2000):

$$C_V = \frac{\alpha K V}{\gamma_{th}} \quad (11)$$

This formulation contains no asymptotic limit and so may represent a more realistic model under high-temperature conditions. If it is again assumed that $\gamma_{th} = \gamma$ and that K is athermal (i.e. $K = K_0$), Equation 5 may be used to derive an expression for C_v without requiring the bulk modulus or a Grüneisen parameter:

$$C_V = \frac{\alpha V Q}{V_0} \quad (12)$$

Neither value for C_v is directly comparable to experimental measurements of heat capacity which are made at constant pressure. The constant pressure or isobaric heat capacity (C_P) is related to the volumetric heat capacity as follows:

$$\left(\frac{C_P}{C_V}\right) = 1 + \gamma_{th}\alpha T \quad (13)$$

Again, by assuming the Grüneisen parameters in Equations 5, and 11, 13 are the same C_P is calculable.

Figure 8 plots the calculated isobaric heat capacities for the three phases studied here along with previous data. At temperatures greater than ~ 300 K the heat capacities derived using equation 12 become significantly greater than those from the simple Debye approximation (Equation 10). Our calculated values for the heat capacity derived directly from the Debye model (i.e. via Equation 10) are greater than the measured values of Ashida et al. (1985). At higher temperatures, though, the calculated heat capacities of Ross and Navrotsky (1988) are slightly smaller than our Debye-derived values at 298 K and are very close above 600 K. Below ~850 K, Ross and Navrotsky (1988) and our Debye heat capacities agree that C_p(clinopyroxene-structured $MgGeO_3$) > C_p(orthopyroxene-structured $MgGeO_3$) > C_p(ilmenite-structured $MgGeO_3$). The heat capacities derived from Equation 12 also have this condition below ~485 K. Above 635 K, these heat capacities have C_p(clinopyroxene-structured $MgGeO_3$) > C_p(ilmenite-structured $MgGeO_3$) > C_p(orthopyroxene-structured $MgGeO_3$), with the lower orthopyroxene phase heat capacity related to the smaller thermal expansion of the orthopyroxene phase relative to the other phases. This concords with the observations showing that, at less than 25 K in $MgSiO_3$, the heat capacity of clinopyroxene is greater than orthopyroxene (Drebushchak et al. 2008). It is clear from Figure 8 that the available experimental heat capacity data seem better matched by values we have obtained via Equation 10 and that the approximations inherent in Equation 12 may, therefore, be leading to an overestimate of C_p. However, Fiquet et al. (1992), have reported experimental values of C_p for other germanates at high temperature that exceed the value from the Dulong-Petit law by similar

amounts to that shown in Figure 8, e.g. by up to 13% for olivine-structured Mg_2GeO_4 and 30% for olivine-structured $CaMgGeO_4$.

Insert Figure 8 here.

Thermodynamic Clapeyron slope

The Clapeyron slope of a phase boundary is given by:

$$\frac{\mathrm{d}P}{\mathrm{d}T} = \frac{\Delta S}{\Delta V} \qquad 14$$

where ΔS and ΔV are the entropy and volume change across the phase transition. The entropy of a mineral is related to its heat capacity by:

$$\left(\frac{\partial S}{\partial T}\right)_P = \frac{C_P}{T} \qquad 15$$

and, therefore, the thermophysical parameters calculated above are sufficient to estimate the Clapeyron slope of the boundary - provided that an adequate representation of C_p can be obtained from the thermal expansion measurements. For any set of isobaric measurements, the result will be the value of the Clapeyron slope as a function of temperature along the isobar. In the present work, the thermal expansion measurements have all been made at ambient pressure and so the calculated slope will be that of the phase boundary at the point where it crosses the temperature axis in Figure 3. Thermodynamics requires that the Clapeyron slope must fall to zero as T approaches 0 K; for finite temperatures, in cases where the Clapeyron slope shows a strong temperature dependence, it then will be necessary to know the temperature of the phase boundary to calculate the correct value of the Clapeyron slope. As a result, the method described here provides only a check on the correctness of the slopes of phase boundaries, rather than a method

554 for determining their absolute position in P-T space. The Clapeyron slopes, calculated using both
555 representations of the heat capacities (Equations 10 and 12) for each phase transition, are plotted
556 in Figure 9. The Clapeyron slopes at the 0 GPa intersection temperature are listed in Table 2.
557

Insert Figure 9 here.

558

559 Below ~300 K, there is little difference between Clapeyron slopes however they are
560 calculated but above this temperature the possible Clapeyron slopes show a wider range depending
561 on the assumed heat capacity (Figure 9). At high temperatures, Clapeyron slopes calculated with
562 heat capacities directly from the Debye model (Equation 10) show asymptotic behaviour which is
563 not present in Clapeyron slopes calculated using Equation 12. This is because the heat capacity
564 from the Debye model asymptotes to the classical limit. With Debye-model heat capacities, the
565 Clapeyron slope of the orthopyroxene-clinopyroxene phase boundary is always positive but when
566 Equation 12 is used the Clapeyron slope is negative at temperatures greater than 1665 K (Figure
567 9a). At 1736 K, where our orthopyroxene-clinopyroxene phase boundary intersects 0 GPa, the
568 calculated Clapeyron slope is -1.8 MPa/K. For the clinopyroxene-ilmenite phase transition, the use
569 of heat capacities obtained from Equation 12 increases the calculated Clapeyron slope but it
570 remains somewhat less than the experimental values of either Kirfel and Neuhaus (1974) or that
571 found in the present work (Figure 9b). However, when it is considered that these Clapeyron slopes
572 are calculated from 0 GPa data and that there are a number of simplifying assumptions in the
573 calculations, we believe that they strongly support conclusion that our phase boundaries as
574 determined by direct high-P/T experiments are correct.
575

Discussion

In this study, the experimental phase diagram is in excellent agreement with that of Kirfel and Neuhaus (1974). Both studies find a negative Clapeyron slope for the orthopyroxene-clinopyroxene phase boundary and the orthopyroxene-clinopyroxene-ilmenite phase triple point close to 0.98 GPa and 752 K. This topology is different from the $MgSiO_3$ system, in which the Clapeyron slope of the orthopyroxene-clinopyroxene transition is positive and there is no equivalent triple point. There is no evidence for a low-temperature $P2_1/c$ clinopyroxene-structured $MgGeO_3$ phase and it is not required by the phase diagram. However, it may be kinetically inhibited from forming below ~900 K but this seems unlikely given that in $MgSiO_3$ the $P2_1/c$ clinopyroxene forms spontaneously during decompression of the $C2/c$ clinopyroxene. The phase diagram is also consistent with orthopyroxene-structured $MgGeO_3$ transforming directly to the $C2/c$ clinopyroxene phase above 1828 K at 0 GPa. There is no significant break in slope of the orthopyroxene-clinopyroxene phase boundary (Figure 1a) that may indicate the presence of the protopyroxene (*Pbcn*) structure argued for by Ozima and Akimoto (1983). Although its presence cannot be excluded, if it does exist, it is likely to have only a small narrow, high temperature, stability field.

Our experimental phase diagram, and that of Kirfel and Neuhaus (1974), are consistent with the thermophysical property measurements if the heat capacity exceeds the Dulong-Petit limit (Equation 12). In this case the heat capacity estimated for the clinopyroxene phase increases faster than that of the orthopyroxene phase (Figure 8). The associated relative increase in the entropy of the clinopyroxene phase at high temperatures changes the Clapeyron slope (Equation 14), expanding the phase field at the expense of the orthopyroxene phase. Although the heat capacity of ilmenite-structured $MgGeO_3$ (Figure 8) is consistent with the Dulong-Petit limit, and would thus

599 have negligible anharmonicity, assuming heat capacities calculated using Equation 12 leads to
600 Clapeyron slopes that correspond better to the phase boundaries determined by direct experiment.
601 There are no measurements of heat capacity in germanate pyroxenes with which we can compare
602 our estimates, but heat capacities well above the Dulong-Petit limit have been observed in
603 germanate olivines (Fiquet et al. 1992) and significant anharmonicity has been observed in
604 germanate perovskites (Andrault et al. 2015). The prevalence of anharmonicity more generally in
605 germanate oxides points to it being present in the phases here and the cause of their apparently
606 increased heat capacity. We note, though, that other processes can cause increases in heat capacity
607 at high temperature, e.g. defect formation (Pamato et al., 2018).

608 Whatever is assumed about the heat capacity, for the clinopyroxene-ilmenite phase
609 transition, our results are in broad agreement with those of Ross and Navrotsky (1988). Our phase
610 diagram and interpretation of the thermophysical properties, though, disagrees with their results
611 for the orthopyroxene-clinopyroxene phase boundary.

612 Although anharmonicity and/or significant formation of defects in clinopyroxene-
613 structured $MgGeO_3$ can reconcile the experimental observations, there is another factor that may
614 explain the discrepancies, between studies, namely an extremely small transformation shear-stress
615 between clinopyroxene and orthopyroxene-structured phases. The possibility that the low-pressure
616 extent of the clinopyroxene phase field is controlled by shear-stress controlled back-transformation
617 has been presented before (Ringwood and Seabrook 1962) and has been observed during
618 deformation of natural pyroxenes (Coe and Kirby 1975). It is unlikely, though, that this effect has
619 any effect on the phase diagram here because (a) our phase boundary is in almost perfect agreement
620 with that of Kirfel and Neuhaus (1974) and (b) the clinopyroxene-structured $MgGeO_3$ samples

621 were ground prior to the thermal expansion measurements and no back transformation was
622 observed in the sample.
623
624 **Implications**
625 Based on the evidence in this study, we suggest that $MgGeO_3$ polymorphs and the clinopyroxene
626 in particular may be significantly more anharmonic than the equivalent $MgSiO_3$ polymorphs. This
627 observation unifies the experimental observations of the phase boundaries; however, there are
628 currently no heat capacity measurements against which to test this assertion. Therefore, to fully
629 understand the system more thermophysical property measurements and/or *in-situ* experiments
630 must be performed.
631 The presence of potentially significant anharmonicity in clinopyroxene-structured
632 $MgGeO_3$, magnesium germanates (e.g. Fiquet et al. 1992) and germanates more generally (e.g.
633 Andrault et al. 2015), is a major difference between the germanate and silicate systems. These
634 effects must therefore be considered when using germanates as low-pressure analogues for Earth
635 forming minerals, especially at elevated temperatures.
636
637 **Acknowledgements**
638 SAH (NE/L006898/1, NE/P017525/1), JRS and DPD (NE/K002902/1) thank the Natural
639 Environment Research Council for funding. IGW thanks the Science and Technology Facilities
640 Council (ST/K000934/1) for funding. This work is based on the PhD thesis work of JRS
641 (University College London, 2017).
642
643 **References**

644 Akaogi, M., Ito, E., and Navrotsky, A. (1989) Olivine-modified spinel-spinel transitions in the
645 system Mg 2 SiO 4 -Fe 2 SiO 4 : Calorimetric measurements, thermochemical calculation,
646 and geophysical application. Journal of Geophysical Research: Solid Earth, 94, 15671–
647 15685.
648 Akaogi, M., Kojitani, H., Yusa, H., Yamamoto, R., Kido, M., and Koyama, K. (2005) High-
649 pressure transitions and thermochemistry of MGeO3 (M=Mg, Zn and Sr) and Sr-silicates:
650 Systematics in enthalpies of formation of A2+B4+O3 perovskites. Physics and Chemistry
651 of Minerals, 32, 603–613.
652 Angel, R.J., and Hugh-Jones, D.A. (1994) Equations of state and thermodynamic properties of
653 enstatite pyroxenes. Journal of Geophysical Research, 99, 777–783.
654 Angel, R.J., and Jackson, J.M. (2002) Elasticity and equation of state of orthoenstatite, MgSiO3.
655 American Mineralogist, 87, 558–561.
656 Ashida, T., Miyamoto, Y., and Kume, S. (1985) Heat capacity, compressibility and thermal
657 expansion coefficient of ilmenite-type MgGeO3. Physics and Chemistry of Minerals, 12,
658 129–131.
659 Boyd, F.R., and England, J.L. (1960) Apparatus for phase-equilibrium measurements at
660 pressures up to 50 kilobars and temperatures up to 1750°C. Journal of Geophysical
661 Research, 65, 741.
662 Coe, R.S., and Kirby, S.H. (1975) The orthoenstatite to clinoenstatite transformation by shearing
663 and reversion by annealing: Mechanism and potential applications. Contributions to
664 Mineralogy and Petrology, 52, 29–55.
665 Drebushchak, V.A., Kovalevskaya, Y.A., Paukov, I.E., and Surkov, N. V. (2008) Low-
666 temperature heat capacity of monoclinic enstatite. Journal of Thermal Analysis and

667 Calorimetry, 94, 493–497.
668 Fiquet, G., Gillet, P., and Richet, P. (1992) Anharmonicity and high-temperature heat capacity of
669 crystals: the examples of Ca2GeO4, Mg2GeO4 and CaMgGeO4 olivines. Physics and
670 Chemistry of Minerals, 18, 469–479.
671 Hirose, K., Kawamura, K., Ohishi, Y., Tateno, S., and Sata, N. (2005) Stability and equation of
672 state of MgGeO3 post-perovskite phase. American Mineralogist, 90, 262–265.
673 Hölzer, G., Fritsch, M., Deutsch, M., Härtwig, J., and Förster, E. (1997) K a1,2 and K b1,3 x-ray
674 emission lines of the 3d transition metals. Physical Review A, 56, 4554–4568.
675 Hugh-Jones, D. (1997) Thermal expansion of MgSiO3 and FeSiO3 ortho- and clinopyroxenes.
676 American Mineralogist, 82, 689–696.
677 Hunt, S.A., Wann, E.T.H., Dobson, D.P., Vočadlo, L., and Wood, I.G. (2017) The thermal
678 expansion of (Fe 1− y Ni y)Si. Journal of Physics: Condensed Matter, 29, 335701.
679 Ito, E., and Matsui, Y. (1979) High-pressure transformations in silicates, germanates, and
680 titanates with ABO3 stoichiometry. Physics and Chemistry of Minerals, 4, 265–273.
681 Kirfel, A., and Neuhaus, A. (1974) Zustandsverhalten und elektrische Leitfähigkeit von MgGeO
682 3 bei Drücken bis 65 kbar und Temperaturen bis 1300°C (mit Folgerungen für das
683 Druckverhalten von MgSiO 3). Zeitschrift für Physikalische Chemie, 91, 121–152.
684 Kirfel, A., Hinze, E., and Will, G. (1978) The rhombohedral high pressure phase of MgGeO3
685 (Ilmenite): Synthesis and single crystal structure analysis. Zeitschrift fur Kristallographie -
686 New Crystal Structures, 148, 305–317.
687 Knight, K.S., and Price, G.D. (2008) Powder neutron-diffraction studies of clinopyroxenes. I.
688 The crystal structure and thermoelastic properties of jadeite between 1.5 and 270 K.
689 Canadian Mineralogist, 46, 1593–1622.

690 Knittle, E. (1995) Static Compression Measurements of Equations of State. In T.J. Ahrens, Ed.,
691 Mineral Physics & Crystallography: A Handbook of Physical Constants, Volume 2 pp. 98–
692 142. American Geophysics Union.
693 Kostiner, E., and Bless, P.W. (1971) Magnesium Germanate and Fluorogermanate. Journal of
694 The Electrochemical Society, 118, 351.
695 Larson, A.C., and Von Dreele, R.B. (2000) General Structure Analysis System, 86–748 p.
696 Laubengayer, A.W., and Morton, D.S. (1932) GERMANIUM. XXXIX. THE
697 POLYMORPHISM OF GERMANIUM DIOXIDE 1. Journal of the American Chemical
698 Society, 54, 2303–2320.
699 Le Bail, A., Duroy, H., and Fourquet, J.L. (1988) Ab-initio structure determination of LiSbWO6
700 by X-ray powder diffraction. Materials Research Bulletin, 23, 447–452.
701 Leinenweber, K., Yanbin Wang, Yagi, T., and Yusa, H. (1994) An unquenchable perovskite
702 phase of MgGeO3 and comparison with MgSiO3 perovskite. American Mineralogist, 79,
703 197–199.
704 Liebermann, R.C. (1974) Elasticity of pyroxene-garnet and pyroxene-ilmenite phase
705 transformations in germanates. Physics of the Earth and Planetary Interiors, 8, 361–374.
706 Lindemann, W. (1961) The unit cell and space group of MgGeO3. Acta Crystallographica, 14,
707 998–998.
708 Lindsay-Scott, A., Wood, I.G., and Dobson, D.P. (2007) Thermal expansion of CaIrO3
709 determined by X-ray powder diffraction. Physics of the Earth and Planetary Interiors, 162,
710 140–148.
711 Lyon, S.R. (1968) Phase Reactions in the systems MgO-SiO2- MgF2, MgO-GeO2-MgF2, and
712 MgO-GeO2-Mg(OH)2. Ohio State Univeristy.

McCormick, G.R. (1964) An investigation of the compatbility relations in the system MgO-GeO-MgF2-LiF principally at 1000°C. Ohio State University.

Murakami, T., Takeuchi, Y., and Yamanaka, T. (1982) The transition of orthoenstatite to protoenstatite and the structure at 1080 °C. Zeitschrift fur Kristallographie - New Crystal Structures, 160, 299–312.

Oganov, A.R., and Dorogokupets, P.I. (2004) Intrinsic anharmonicity in equations of state and thermodynamics of solids. Journal of Physics Condensed Matter, 16, 1351–1360.

Ohi, S., and Miyake, A. (2016) Phase transitions between high- and low-temperature orthopyroxene in the Mg2Si2O6 -Fe2Si2O6 system. American Mineralogist, 101, 1414–1422.

Okada, T., Narita, T., Nagai, T., and Yamanaka, T. (2008) Comparative Raman spectroscopic study on ilmenite-type MgSiO3 (akimotoite), MgGeO3, and MgTiO3 (geikielite) at high temperatures and high pressures. American Mineralogist, 93, 39–47.

Ozima, M. (1983) Structure of orthopyroxene-type and clinopyroxene-type magnesium germanium oxide MgGeO3. Acta Crystallographica, C39, 1169–1172.

Ozima, M., and Akimoto, S.I. (1983) Flux growth of single crystals of MgGeO3 polymorphs (orthopyroxene, clinopyroxene, and ilmenite) and their phase relations and crystal structures. American Mineralogist, 68, 1199–1205.

Pamato, M.G., Wood, I.G., Dobson, D.P., Hunt, S.A., and Vočadlo, L. (2018) The thermal expansion of gold: point defect concentrations and pre-melting in a face-centred cubic metal. Journal of Applied Crystallography, 51, 470–480.

Poirier, J.-P. (2000) Introduction to the Physics of the Earth's Interior. Cambridge University Press.

Redhammer, Günther Josef, Senyshyn, A., Tippelt, G., Pietzonka, C., Roth, G., and Amthauer, G. (2010) Magnetic and nuclear structure and thermal expansion of orthorhombic and monoclinic polymorphs of CoGeO3 pyroxene. Physics and Chemistry of Minerals, 37, 311–332.

Redhammer, Günther J., Cámara, F., Alvaro, M., Nestola, F., Tippelt, G., Prinz, S., Simons, J., Roth, G., and Amthauer, G. (2010) Thermal expansion and high-temperature P21/c-C2/c phase transition in clinopyroxene-type LiFeGe2O6 and comparison to NaFe(Si,Ge)2O6. Physics and Chemistry of Minerals, 37, 685–704.

Rietveld, H.M. (1969) A profile refinement method for nuclear and magnetic structures. Journal of Applied Crystallography, 2, 65–71.

Ringwood, A.E., and Seabrook, M. (1962) High-pressure transition of MgGeO3 from pyroxene to corundum structure. Journal of Geophysical Research, 67, 1690–1691.

Robbins, C.R., and Levin, E.M. (1959) The system magnesium oxide-germanium dioxide. American Journal of Science.

Ross, N.L., and Navrotsky, A. (1987) The Mg2GeO4 olivine-spinel phase transition. Physics and Chemistry of Minerals, 14, 473–481.

Ross, N.L., and Navrotsky, A. (1988) Study of the MgGeO3 polymorphs (orthopyroxene, clinopyroxene, and ilmenite structures) by calorimetry, spectroscopy, and phase equilibria. American Mineralogist, 73, 1355–1365.

Roth, R.S. (1955) Synthetic Alkaline Earth Germinates Isostructural with Enstatite and Pseudowollastonite. American Mineralogist, 40, 322.

——— (1957) Classification of perovskite and other ABO3-type compounds. Journal of Research of the National Bureau of Standards, 58, 75.

759 Sarver, J.F., and Hummel, F.A. (1963) Subsolidus Equilibria and Luminescence Data on Phases
760 in the System MgO-GeO[sub 2]-SiO[sub 2]-TiO[sub 2]. Journal of The Electrochemical
761 Society, 110, 726.
762 Sato, Y., Ito, E., and Akimoto, S. iti (1977) Hydrostatic compression of ilmenite phase of
763 ZnSiO3 and MgGeO3. Physics and Chemistry of Minerals, 2, 171–176.
764 Thompson, P., and Wood, I.G. (1983) X-ray Rietveld refinement using Debye–Scherrer
765 geometry. Journal of Applied Crystallography, 16, 458–472.
766 Toby, B.H. (2001) EXPGUI, a graphical user interface for GSAS. Journal of Applied
767 Crystallography, 34, 210–213.
768 Tsuchiya, T., and Tsuchiya, J. (2007) High-pressure-high-temperature phase relations of MgGe
769 O3: First-principles calculations. Physical Review B - Condensed Matter and Materials
770 Physics, 76, 2–5.
771 Ulmer, P., and Stalder, R. (2001) The Mg(Fe)SiO3 orthoenstatite-clinoenstatite transitions at
772 high pressures and temperatures determined by Raman-spectro scopy on quenched samples.
773 American Mineralogist, 86, 1267–1274.
774 Vegard, L. (1932) Die Struktur von β-Stickstoff und die verschiedene Phosphoreszenzfähigkeit
775 der beiden Formen des festen Stickstoffs. Zeitschrift für Physik, 79, 471–491.
776 Vočadlo, L., Knight, K.S., Price, G.D., and Wood, I.G. (2002) Thermal expansion and crystal
777 structure of FeSi between 4 and 1173 K determined by time-of-flight neutron powder
778 diffraction. Physics and Chemistry of Minerals, 29, 132–139.
779 von Dreele, R.B., Bless, P.W., Kostiner, E., and Hughes, R.E. (1970) The crystal structure of
780 magnesium germanate: A reformulation of Mg4GeO6 as Mg28Ge10O48. Journal of Solid
781 State Chemistry, 2, 612–618.

782 Walker, D., Carpenter, M.A., and Hitch, C.M. (1990) Some simplifications to multianvil devices
783 for high pressure experiments. American Mineralogist, 75, 1020–1028.
784 Wallace, D.C. (1998) Thermodynamics of crystals. Dover Publications, Mineola, N.Y.
785 Wood, I.G., Dominic Fortes, A., Dobson, D.P., Wang, W., Pajdzik, L., and Cosier, J. (2018)
786 Investigation of high-pressure planetary ices by cryo-recovery. I. an apparatus for X-ray
787 powder diffraction from 40 to 315 k, allowing 'cold loading' of samples. Journal of Applied
788 Crystallography, 51, 685–691.
789 Yamanaka, T., Hirano, M., and Takeuchi, Y. (1985) A high temperature transition in MgGeO3
790 from clinopyroxene (C2/c) type to orthopyroxene (Pbca) type. American Mineralogist, 70,
791 365–374.
792 Yamanaka, T., Komatsu, Y., Sugahara, M., and Nagai, T. (2005) Structure change of MgSiO3,
793 MgGeO3, and MgTiO3 ilmenites under compression. American Mineralogist, 90, 1301–
794 1307.
795 Yang, H., and Ghose, S. (1994) Thermal expansion, Debye temperature and Grüneisen parameter
796 of synthetic (Fe, Mg)SiO3 orthopyroxenes. Physics and Chemistry of Minerals, 20, 575–
797 586.
798

Figure 1. Phase diagrams and synthesis conditions in the $MgGeO_3$ system from previous studies. Large symbols are data from (a) Kirfel and Neuhaus (1974) (b) Ross and Navrotsky (1988) and (c) Ozima and Akimoto (1983). Small symbols in (b) are synthesis conditions reported by Roth (1955); Ringwood and Seabrook (1962); Liebermann (1974); Sato et al. (1977); Kirfel et al. (1978); Ito and Matsui (1979); Ashida et al. (1985); Okada et al. (2008). Symbols: □ – orthopyroxene, o – clinopyroxene, △ - ilmenite, ▽ – protopyroxene; open – forward and filled - reversals, except data of Ross and Navrotsky (1988) (b) where all experiments started with both clinopyroxene and ilmenite so are both forward and reverse. Solid lines are phase boundaries in reference, dotted lines in (b), (c) are the clinopyroxene—ilmenite phase boundary of Kirfel and Neuhaus (1974) for comparison.

Figure 2. Sample X-ray powder diffraction patterns showing the observations (points), calculated fit (upper line) and difference (lower trace) for (a) clinopyroxene and ilmenite $MgGeO_3$ and (b) orthopyroxene $MgGeO_3$ at 298 K. The tick marks show the positions of the Bragg reflections from (a) clinopyroxene, MgO and ilmenite (top to bottom) and (b) MgO and orthopyroxene.

F*igure 3. (a) $MgGeO_3$ phase diagram from the experiments in this study and (b) comparison of our phase boundaries (bold solid line) with those of Kirfel and Neuhaus (1974; solid line), Ozima and Akimoto (1983; dashed line) and Ross and Navrotsky (1988; dotted line). Symbols: □ – orthopyroxene, o – clinopyroxene, △ - ilmenite; open – forward and filled – reversals. Small symbols denote experiments that were kinetically inhibited. Coloured regions in (b) are the extent of the phase fields constrained by our experiments*

Figure 4: (top) Lattice parameters, unit-cell volumes and (bottom) residuals to fit of orthopyroxene $MgGeO_3$ (Table 3), normalised to the 0 K values reported in Table 5. The error bars are omitted for clarity and the high-temperature measurements are multiplied by the scale factor. Lines are normalised fits of the Debye-Grüneisen model to the data of this study. Filled symbols are the data from Yamanaka et al. (1985).

Figure 5. (top) Lattice parameters, unit-cell volumes and (bottom) residuals to fit of clinopyroxene $MgGeO_3$ (Table 3), normalised to the 0 K values reported in Table 5. The error bars are omitted for clarity and the high-temperature measurements are multiplied by the scale factor. Lines are normalised fits of the Debye-Grüneisen model to the data of this study. Filled symbols are the data from Yamanaka et al. (1985).

Figure 6. (top) Lattice parameters, unit-cell volumes and (bottom) residuals to fit of ilmenite $MgGeO_3$ (Table 3), normalised to the 0 K values reported in Table 5. The error bars are omitted for clarity and the high-temperature measurements are multiplied by the scale factor. Lines are normalised fits of the Debye-Grüneisen model to the data of this study. Filled symbols are the data from Ashida et al. (1985).

Figure 7. Volumetric thermal expansivity of $MgGeO_3$ phases. Lines and symbols as in the legend.

Figure 8. Calculated isobaric heat capacities of $MgGeO_3$ phases, converted from isovolumetric heat capacities (equation 13). Lines and symbols as in the legend. The Horizontal dashed grey line is the Dulong-Petit limit for the heat capacity at constant volume.

Figure 9. Clapeyron slopes of the (a) orthopyroxene-clinopyroxene and (b) clinopyroxene-ilmenite phase transitions. Lines and symbols as in the legends.

Expt.	Type	Pressure	Temperature	Duration	Sample	
		(GPa)	(K)	(hours)	starting	recovered
synthesis	furnace	1 bar	1373	72	oxides	opx
synthesis	MA	2.5	1173	3	opx	cpx
synthesis	MA	5.0	1273	3	opx	ilm
GER001	MA	2.1	1273	2	opx	cpx
GER003	MA	3.6	1173	3	opx	cpx
GER004	MA	2.6	1273	1.33	opx	cpx
GER005	MA	3.3	1273	1.5	opx	cpx
GER006	MA	4.6	1273	1.5	opx	ilm
GER007	MA	1.3	1073	1.5	opx	cpx+opx
GER008$	MA	2.0	823	3	opx	cpx
GER011$	MA	2.6	823	20	opx	cpx
GER012	MA	3.9	1273	3	opx	cpx
GER013#	MA	4.2	1273	3	opx	cpx
GER014	MA	3.1	1123	3	opx	cpx
GER015$	MA	3.0	823	3	opx	cpx
GER017	MA	3.6	1123	3	opx	1:9 cpx:ilm
GER018#	MA	3.1	1073	1	opx	9:1 cpx:ilm
GER019	MA	2.9	1073	3	opx	cpx
GER020#	MA	3.3	1123	1	opx	cpx
GER022	MA	6.1	1523	2	opx	ilm
GER024#	MA	5.6	1473	2.66	opx	ilm
GER025	MA	5.4	1493	3	opx	cpx
GER028	MA	2.5	973	3	opx	cpx+ilm
GER029#	PC	0.6	973	24	opx	opx
GER031#	PC	0.9	973	24	opx	cpx
GER032	PC	0.9	1323	4.5	opx	cpx
GER033	PC	1.2	1323	3	opx	cpx
GER035#	PC	0.3	1323	17.5	opx	opx
GER037#	PC	0.6	1273	3	opx	cpx+opx
GER042	MA	5.0	1273	3	opx	ilm
GER043	MA	5.0	1273	3	opx	ilm
GER044	MA-R	3.0	1123	3.5	ilm	ilm+cpx
GER046	MA-R	3.9	1273	3.5	ilm	ilm+cpx

Table 1. Experimental conditions and outcomes used here to synthesise samples and constrain the phase diagram. PC – piston cylinder experiment, MA – multi-anvil, MA-R – reversal. Samples: opx – orthopyroxene, cpx – clinopyroxene and ilm – ilmenite. The experiments that are used to calculate the phase boundary positions are denoted by # and those inferred to be kinetically inhibited are denoted by $.

Author	Type	Clapeyron Slope (MPa/K)	ΔS (J/K/mol)
Orthopyroxene – clinopyroxene			
This study	Experimental	$-1.0^{+1.0}_{-0.7}$	1.17 [a]
Kirfel and Neuhaus (1974)	Experimental	-0.82	0.96 [a]
Ozima and Akimoto (1983)	Experimental	28	-32.69 [a]
Ross and Navrotsky (1988)	Calorimetry	2.1	-3
This study	Calculated (Debye, 1736 K)	16.0(0) [b]	-15.67(1)
This study	Calculated (αT, 1736 K)	-1.76(0) [b]	1.72(6)
Clinopyroxene – ilmenite			
This study	Experimental	$6.4^{+1.0}_{-0.6}$	-23.55 [a]
Kirfel and Neuhaus (1974)	Experimental	5.45	-19.98 [a]
Ross and Navrotsky (1988)	Calorimetry	2.0(4)	-7.6(15)
This study	Calculated (Debye, 600 K)	2.8(0) [b]	-10.34(7)
This study	Calculated (αT, 600 K)	3.1(0) [b]	-11.53(9)

Table 2. Clapeyron slopes of the phase boundaries reported here and in previous studies. The Calculated Clapeyron slopes are reported at the temperature of the experimental phase boundary at 0 GPa; for the temperature evolution of the calculated Clapeyron slopes see Figure 9. The heat capacities used to calculate the Clapeyron slope were either the Debye heat capacity (Equation 10) or the anharmonic heat capacity (αT, Equations 11, 12); see text for details. a. ΔS values are calculated using the ΔV from the thermal expansion measurements in this study at 900 K. b. Errors are $<5 \times 10^{-4}$ but greater than zero.

Temperature	Orthopyroxene (*Pbca*)				Clinopyroxene (*C*2/*c*)					Ilmenite ($R\bar{3}$)		
(K)	Volume (Å^3)	a (Å)	b (Å)	c (Å)	Volume (Å^3)	a (Å)	b (Å)	c (Å)	β (º)	Volume (Å^3)	a (Å)	c (Å)
Low temperature stage												
40	897.40(3)	18.7970(3)	8.9438(2)	5.33798(9)	433.156(8)	9.58991(8)	8.92315(7)	5.15484(4)	100.898(1)	289.134(5)	4.93239(5)	13.72313(15)
60	897.25(2)	18.7966(3)	8.9432(2)	5.33753(9)	433.181(7)	9.59022(7)	8.92339(7)	5.15485(4)	100.899(1)	289.150(5)	4.93246(4)	13.72352(14)
80	897.41(2)	18.7979(3)	8.9439(2)	5.33773(9)	433.197(8)	9.59042(8)	8.92348(7)	5.15491(4)	100.900(1)	289.151(5)	4.93242(4)	13.72378(14)
100	897.48(2)	18.7979(3)	8.9443(2)	5.33786(9)	433.282(7)	9.59116(7)	8.92414(7)	5.15524(4)	100.906(1)	289.198(5)	4.93270(4)	13.72448(14)
120	897.66(2)	18.7989(3)	8.9450(2)	5.33823(9)	433.335(7)	9.59174(8)	8.92467(7)	5.15532(4)	100.910(1)	289.231(5)	4.93290(4)	13.72495(14)
140	897.83(2)	18.8003(3)	8.9457(2)	5.33847(9)	433.431(7)	9.59270(7)	8.92551(7)	5.15555(4)	100.915(1)	289.281(5)	4.93313(4)	13.72598(14)
160	898.13(2)	18.8019(3)	8.9468(2)	5.33914(9)	433.530(7)	9.59370(7)	8.92637(7)	5.15582(4)	100.923(1)	289.331(5)	4.93334(4)	13.72722(14)
180	898.40(2)	18.8035(3)	8.9481(2)	5.33951(9)	433.666(7)	9.59490(7)	8.92760(7)	5.15621(4)	100.930(1)	289.415(5)	4.93376(4)	13.72887(14)
200	898.73(2)	18.8044(3)	8.9496(2)	5.34033(9)	433.797(7)	9.59599(7)	8.92891(7)	5.15656(4)	100.937(1)	289.482(5)	4.93408(4)	13.73025(14)
220	898.95(2)	18.8057(3)	8.9507(1)	5.34053(9)	433.976(7)	9.59770(7)	8.93027(7)	5.15710(4)	100.945(1)	289.592(5)	4.93464(4)	13.73233(14)
240	899.47(2)	18.8086(3)	8.9527(2)	5.34170(9)	434.147(8)	9.59893(8)	8.93187(8)	5.15767(5)	100.952(1)	289.687(5)	4.93512(4)	13.73415(15)
260	899.78(2)	18.8108(3)	8.9536(2)	5.34235(9)	434.311(8)	9.60044(8)	8.93330(8)	5.15815(4)	100.962(1)	289.795(5)	4.93567(4)	13.73625(16)
280	900.19(2)	18.8132(3)	8.9554(2)	5.34301(9)	434.499(8)	9.60203(8)	8.93500(8)	5.15868(4)	100.969(1)	289.896(5)	4.93614(4)	13.73841(15)
300	900.62(2)	18.8153(3)	8.9571(2)	5.34392(9)	434.695(4)	9.60374(4)	8.93675(4)	5.15925(3)	100.978(0)[a]	290.013(3)	4.93671(2)	13.74081(9)
High temperature stage												
298	900.48(2)	18.8149(2)	8.9570(1)	5.34329(7)	434.755(6)	9.60388(6)	8.93706(6)	5.15955(4)	100.969(0)[a]	290.057(4)	4.93703(3)	13.74110(12)
323	901.04(2)	18.8177(2)	8.9594(1)	5.34438(7)	435.015(9)	9.60617(8)	8.93911(8)	5.16041(5)	100.981(1)	290.218(6)	4.93801(5)	13.74328(16)
348	901.59(2)	18.8214(2)	8.9614(1)	5.34542(7)	435.282(9)	9.60845(9)	8.94149(8)	5.16118(5)	100.992(1)	290.374(6)	4.93869(5)	13.74681(16)
373	902.16(2)	18.8245(2)	8.9638(1)	5.34649(7)	435.598(9)	9.61106(9)	8.94406(8)	5.16226(5)	101.004(1)	290.568(6)	4.93970(5)	13.75043(15)
398	902.75(2)	18.8278(2)	8.9662(1)	5.34755(7)	435.884(9)	9.61345(9)	8.94663(8)	5.16309(5)	101.016(1)	290.745(6)	4.94063(5)	13.75363(15)
423	903.37(2)	18.8315(2)	8.9686(1)	5.34876(7)	436.194(9)	9.61621(9)	8.94916(8)	5.16407(5)	101.030(1)	290.939(6)	4.94162(5)	13.75729(15)
448	903.96(2)	18.8348(2)	8.9710(1)	5.34995(7)	436.515(9)	9.61881(9)	8.95191(9)	5.16511(5)	101.043(1)	291.130(6)	4.94261(5)	13.76080(16)
473	904.57(2)	18.8384(2)	8.9734(1)	5.35108(7)	436.840(10)	9.62149(9)	8.95476(9)	5.16610(5)	101.056(1)	291.336(6)	4.94365(5)	13.76475(16)
498	905.20(2)	18.8419(2)	8.9759(1)	5.35232(7)	437.132(9)	9.62386(9)	8.95735(9)	5.16703(5)	101.070(1)	291.511(6)	4.94447(5)	13.76841(15)
523	905.86(2)	18.8460(2)	8.9784(1)	5.35356(7)	437.466(10)	9.62665(9)	8.96023(9)	5.16806(5)	101.084(1)	291.706(6)	4.94545(5)	13.77223(15)
548	906.48(2)	18.8499(2)	8.9808(1)	5.35471(7)	437.777(10)	9.62943(9)	8.96295(9)	5.16897(6)	101.101(1)	291.899(6)	4.94646(5)	13.77566(16)
573	907.12(2)	18.8532(2)	8.9835(1)	5.35594(7)	438.135(11)	9.63240(9)	8.96581(10)	5.17021(6)	101.115(1)	292.125(6)	4.94772(5)	13.77933(16)
598	907.75(2)	18.8570(2)	8.9857(1)	5.35723(7)	438.472(11)	9.63516(10)	8.96886(10)	5.17117(6)	101.129(1)	292.340(7)	4.94883(5)	13.78326(17)
623	908.40(2)	18.8599(2)	8.9880(1)	5.35887(7)	438.848(11)	9.63833(10)	8.97200(10)	5.17240(6)	101.145(1)	292.561(7)	4.94993(6)	13.78760(17)
648	909.05(2)	18.8638(2)	8.9904(1)	5.36015(7)	439.184(12)	9.64100(10)	8.97497(10)	5.17345(6)	101.158(1)	292.767(7)	4.95101(6)	13.79129(17)
673	909.72(2)	18.8683(2)	8.9933(1)	5.36113(7)	439.530(12)	9.64394(11)	8.97798(11)	5.17452(6)	101.176(1)	292.975(8)	4.95208(6)	13.79509(18)
698	910.42(2)	18.8722(2)	8.9961(1)	5.36246(7)	439.902(13)	9.64707(11)	8.98113(11)	5.17565(6)	101.190(1)	293.210(8)	4.95328(6)	13.79945(19)
723	911.11(2)	18.8763(2)	8.9988(1)	5.36380(7)	440.257(13)	9.65001(12)	8.98412(11)	5.17680(7)	101.205(1)	293.420(8)	4.95435(6)	13.80343(18)
748	911.80(2)	18.8796(2)	9.0012(1)	5.36546(7)	440.646(13)	9.65328(12)	8.98734(11)	5.17809(6)	101.223(1)	293.671(8)	4.95564(6)	13.80803(18)
773	912.48(2)	18.8841(2)	9.0040(1)	5.36647(7)	441.048(14)	9.65617(12)	8.99095(12)	5.17944(7)	101.238(1)	293.930(8)	4.95696(6)	13.81284(19)
798	913.16(2)	18.8879(2)	9.0067(1)	5.36781(7)	441.387(14)	9.65935(12)	8.99404(12)	5.18025(7)	101.255(1)	294.126(8)	4.95800(6)	13.81619(19)
823	913.86(2)	18.8920(2)	9.0095(1)	5.36913(7)	441.769(15)	9.66238(13)	8.99703(13)	5.18166(7)	101.271(1)	294.373(8)	4.95923(6)	13.82100(20)
848	914.59(2)	18.8956(2)	9.0120(1)	5.37090(7)	442.171(15)	9.66570(13)	9.00061(12)	5.18287(7)	101.289(1)	294.617(8)	4.96050(6)	13.82538(20)
873	915.34(2)	18.9008(2)	9.0151(1)	5.37193(7)	442.564(15)	9.66900(13)	9.00383(13)	5.18416(7)	101.307(1)	294.863(9)	4.96178(6)	13.82971(20)
898	916.08(2)	18.9049(2)	9.0180(1)	5.37339(7)	442.924(15)	9.67185(13)	9.00704(13)	5.18529(8)	101.322(1)	295.088(9)	4.96291(7)	13.83406(21)
923	916.79(2)	18.9091(2)	9.0207(1)	5.37473(7)	443.323(16)	9.67517(14)	9.01032(13)	5.18661(8)	101.340(1)	295.309(9)	4.96404(7)	13.83804(21)
948	917.55(2)	18.9135(2)	9.0237(1)	5.37619(7)								
973	918.29(2)	18.9175(2)	9.0267(1)	5.37755(7)								
998	919.04(2)	18.9221(2)	9.0294(1)	5.37905(7)								
1023	919.78(2)	18.9262(2)	9.0323(1)	5.38053(7)								
1048	920.58(2)	18.9310(2)	9.0353(1)	5.38205(7)								
1073	921.31(2)	18.9350(2)	9.0381(1)	5.38347(7)								
1098	922.12(2)	18.9397(3)	9.0414(1)	5.38491(8)								
1123	922.90(2)	18.9441(3)	9.0445(1)	5.38636(8)								
1148	923.67(2)	18.9476(2)	9.0473(1)	5.38826(7)								
1173	924.48(2)	18.9518(2)	9.0506(1)	5.38978(7)								
Scale Factor	1.000087	1.000016	0.999979	1.000091	0.999821	0.999968	0.999948	0.999930	1.000079	0.999807	0.999914	0.999978

Table 3. Unit cell parameters and volumes of $MgGeO_3$ phases measured in this study. The numbers in parentheses are one standard error of the least significant digit. Note, however, that the lattice parameter values listed here are probably less accurate than might be expected from the stated uncertainties, which are those reported from the Le Bail

865 *and Rietveld fits using GSAS; for further discussion of the importance of systematic errors in profile refinement of X-ray powder data see e.g.* Thompson and Wood (1983).
866 *Multiplying the high-temperature data by the scale factors aligns it with the low-temperature data; see text for details. a. Errors are* $<5 \times 10^{-4}$ *degrees but greater than zero.*

	Reported temperature	V (Å^3)	a (Å)	b (Å)	c (Å)	β (º)
Orthopyroxene						
This study	298K	900.48(2)	18.8149(2)	8.9570(1)	5.34329(7)	
	300K	900.62(2)	18.8153(3)	8.9571(2)	5.34392(9)	
Roth (1955, 1957)	-	-	18.661	8.954	5.346	
Lyon (1968)	-	-	18.745(5)	8.974(17)	5.350(1)	
Lindemann (1961)	-	-	18.649(7)	8.902(5)	5.332(5)	
Kirfel and Neuhaus (1974)	-	901.17(35)	18.859(6)	8.958(2)	5.334(1)	
Ozima (1983) & Ozima and Akimoto (1983)	-	899.69	18.8099(12)	8.9484(8)	5.3451(4)	
Yamanaka et al. (1985)	20C	901.3(3)	18.829(3)	8.952(2)	5.347(1)	
Clinopyroxene						
This study	298K	434.755(6)	9.60388(6)	8.93706(6)	5.15955(4)	100.969(0)[c]
	300K	434.695(4)	9.60374(4)	8.93675(4)	5.15925(3)	100.978(0)[c]
Kirfel and Neuhaus (1974)	-	440.0(5)	9.623(9) [a]	8.960(5)	5.196(3)	100.144(8)
Ozima (1983) & Ozima and Akimoto (1983)	-	434.27(6)	9.6010(8)	8.9323(6)	5.1592(5)	101.034(9)
Yamanaka et al. (1985)	20C	435.1(1)	9.605(2)	8.940(2)	5.160(1)	100.95(1)
Ilmenite						
This study	298K	290.057(4)	4.93703(3)		13.74110(12)	
	300K	290.013(3)	4.93671(2)		13.74081(9)	
Ringwood and Seabrook (1962)	-	-	4.936(5)		13.76(5)	
Kirfel and Neuhaus (1974)	-	289.8	4.936(1)		13.735(5)	
Kirfel et al. (1978)	-	289.80(14)	4.933(1)		13.734(5)	
Ito and Matsui (1979)	"ambient conditions"	-	4.9363(2)		13.7401(8)	
Ashida et al. (1985)	273K	289.93	-		-	
Tsuchiya and Tsuchiya (2007)	300K	291.48 [b]	4.949 [b]		13.743 [b]	

Table 4. Unit cell parameters from previous studies at ambient conditions. Values not reported are marked '-', numbers in parenthesis are the standard error in the last digit and numbers without parenthesis did not have reported errors. All unit cell parameters were measured by powder or single-crystal X-ray diffraction unless otherwise noted. See note in caption of Table 3 regarding significance of values determined in this study. [a] value was reported as twice this value. [b] calculated using density functional theory. [c] Error is $<5\times10^{-4}$ degrees but greater than 0.

		l_{298K}	a_0 ($\times 10^{-6}$ K^{-1})	a_1 ($\times 10^{-9}$ K^{-2})	a_2 (K)
This study					
Orthopyroxene	volume	900.47402 Å^3	23.46(4)	9.65(7)	-0.169
	a	18.81493(19) Å	7.01(9)	2.22(12)	-0.107
	b	8.95700(7) Å	8.45(7)	4.52(9)	0.034
	c	5.34326(6) Å	7.99(10)	2.92(14)	-0.096
Clinopyroxene	volume	434.75207 Å^3	25.79(15)	11.73(29)	-0.456
	a	9.60388(5) Å	9.89(9)	4.15(16)	-0.157
	b	8.93700(5) Å	11.53(9)	4.19(16)	-0.270
	c	5.15954(3) Å	6.01(11)	4.28(18)	-0.068
	β	100.96923 º	4.95(4)	2.22(7)	-0.120
Ilmenite	volume	290.05569 Å^3	23.32(20)	11.66(39)	-0.429
	a	4.93707(4) Å	6.84(13)	3.89(21)	-0.122
	c	13.74079(14) Å	9.58(16)	3.93(27)	-0.179
Yamanaka et al. (1985)					
Orthopyroxene	volume	901.476(64) Å^3	39.8(1)		
	a	18.830(3) Å	10.1(3)		
	b	8.953(2) Å	15.9(3)		
	c	5.347 Å	13.7(2)		
Clinopyroxene	volume	435.433 Å^3	43.8(132)	-13.4(233)	
	a	9.608(5) Å	16.7(67)	-5.1(104)	
	b	8.944(7) Å	18.4(100)	-5.9(155)	
	c	5.161(2) Å	7.7(54)	4.4(80)	
	β	100.968(36) º	7.9(52)	-1.6(84)	
Ashida et al. (1985)					
Ilmenite	volume	289.816 Å^3	25.7(44)	-2.3(74)	
Tsuchiya and Tsuchiya (2007)					
Ilmenite	volume	291.48 Å^3 a	20.9 a		

Table 5. Polynomial thermal expansion parameters derived from the high-temperature stage data in Table 3, together with selected other data. Numbers in parenthesis are the standard error in the least significant digit; numbers without errors have a standard error of < 0.5 least significant digit. a – 0 GPa, 300 K values calculated using density functional theory.

		l_0	θ_D (K)	Q (x 10^{-16} J)	b	K′	γ
This study, thermal expansion							
Orthopyroxene	volume	897.299(16) Å^3	602(7)	1.199(6)	4.6(1)	10.3(3)	0.861(5)a
	a	18.79709(21) Å	650(16)	4.22(5)	14(1)		
	b	8.94334(11) Å	545(11)	3.11(3)	12(1)		
	c	5.33762(7) Å	635(16)	3.61(5)	13(1)		
Clinopyroxene	volume	433.192(7) Å^3	693(10)	0.56(1)	5.9(4)	12.7(9)	1.01(1)b
	a	9.59029(8) Å	633(12)	1.50(2)	15(1)		
	b	8.92336(6) Å	663(9)	1.36(1	15(1)		
	c	5.15493(3) Å	772(15)	2.03(3)	20(2)		
	β	100.8987(7) º	473(15)	3.47(5)	53(3)		
Ilmenite	volume	289.154(5) Å^3	758(13)	0.44(1)	5.9(5)	12.7(11)	1.23(2)c
	a	4.93251(4) Å	801(18)	1.43(3)	18(2)		
	c	13.72349(10) Å	707(12)	1.13(1)	13(1)		
This study, from experimental Clapeyron slopes							
Clinopyroxene	Orthopyroxene - Clinopyroxene transition						1.07(4)
	Clinopyroxene – Ilmenite transition						1.08(3)
Ashida et al. (1985)							
Ilmenite	volume		819 (all data)			3.6	
			777 (<300K)				
Liebermann (1974)							
Clinopyroxene	volume		618				
Ilmenite	volume		657d				
Tsuchiya and Tsuchiya (2007)							
Ilmenite	volume	291.48 Å^3 e				4.59 e	1.24 e

Table 6. Debye-Grüneisen model thermophysical parameters and derived values. a Calculated using K_T=115 GP; b calculated assuming K_S = 131 GPa; c – calculated using K_T = 187 GPa; d – reported in Okada et al. (2008)*; e – 0 GPa, 300 K values calculated using density functional theory.*

Fig. 1

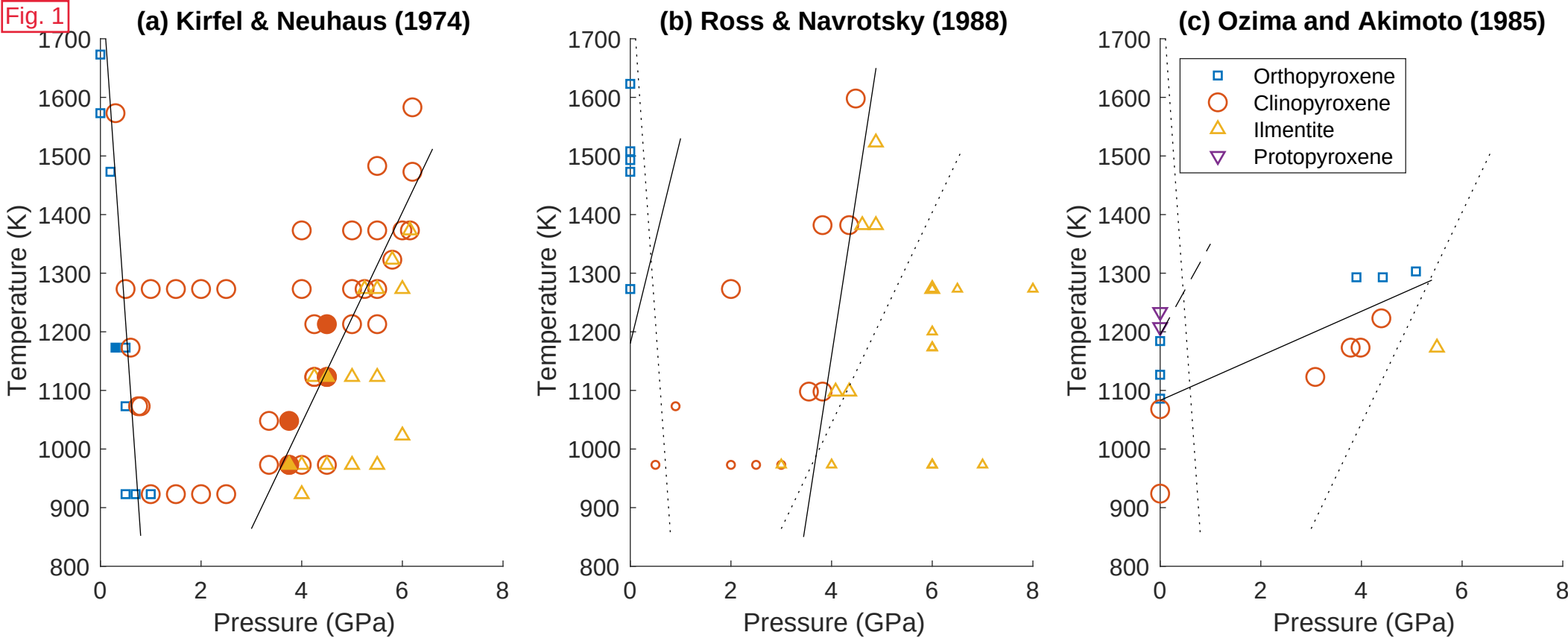
(a) Kirfel & Neuhaus (1974)
(b) Ross & Navrotsky (1988)
(c) Ozima and Akimoto (1985)
Temperature (K)
Pressure (GPa)
Orthopyroxene
Clinopyroxene
Ilmentite
Protopyroxene

Figure 2

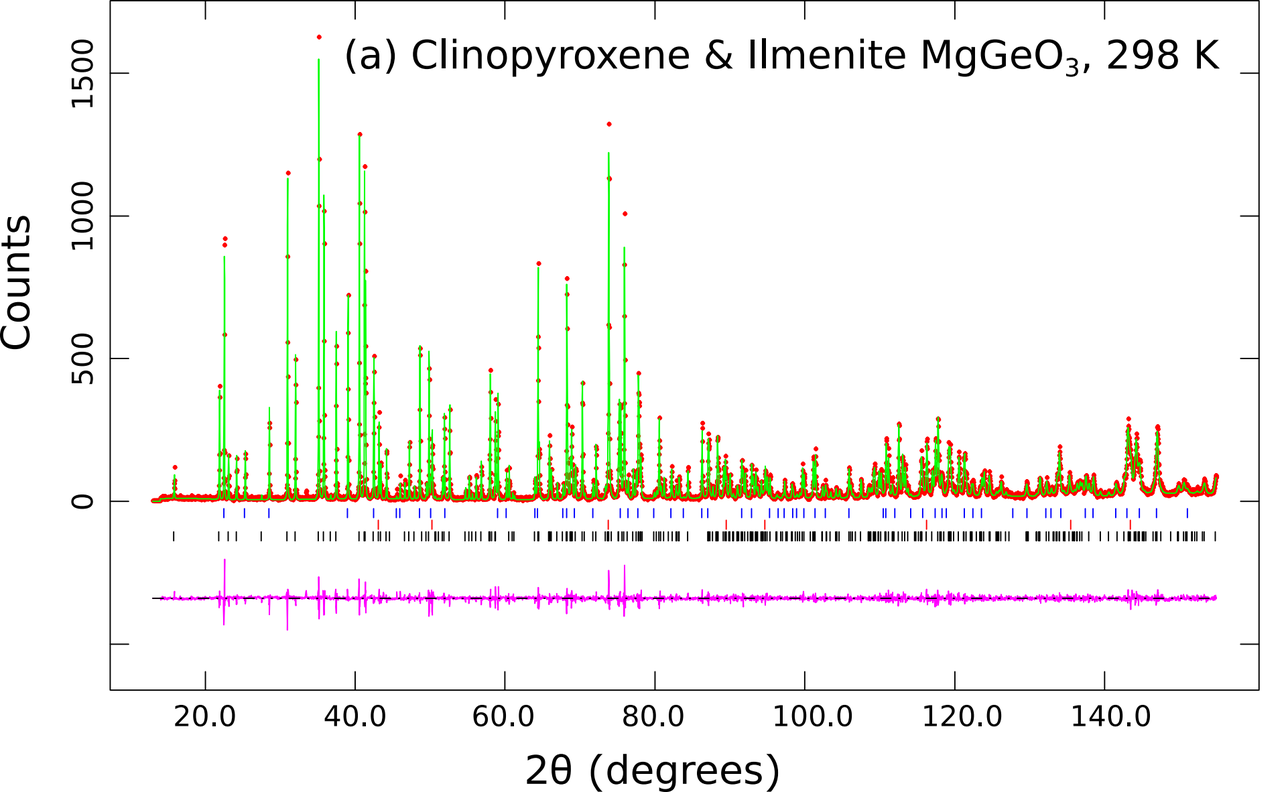
(a) Clinopyroxene & Ilmenite MgGeO3, 298 K
Counts
0
500
1000
1500
20.0
40.0
60.0
80.0
100.0
120.0
140.0
2θ (degrees)

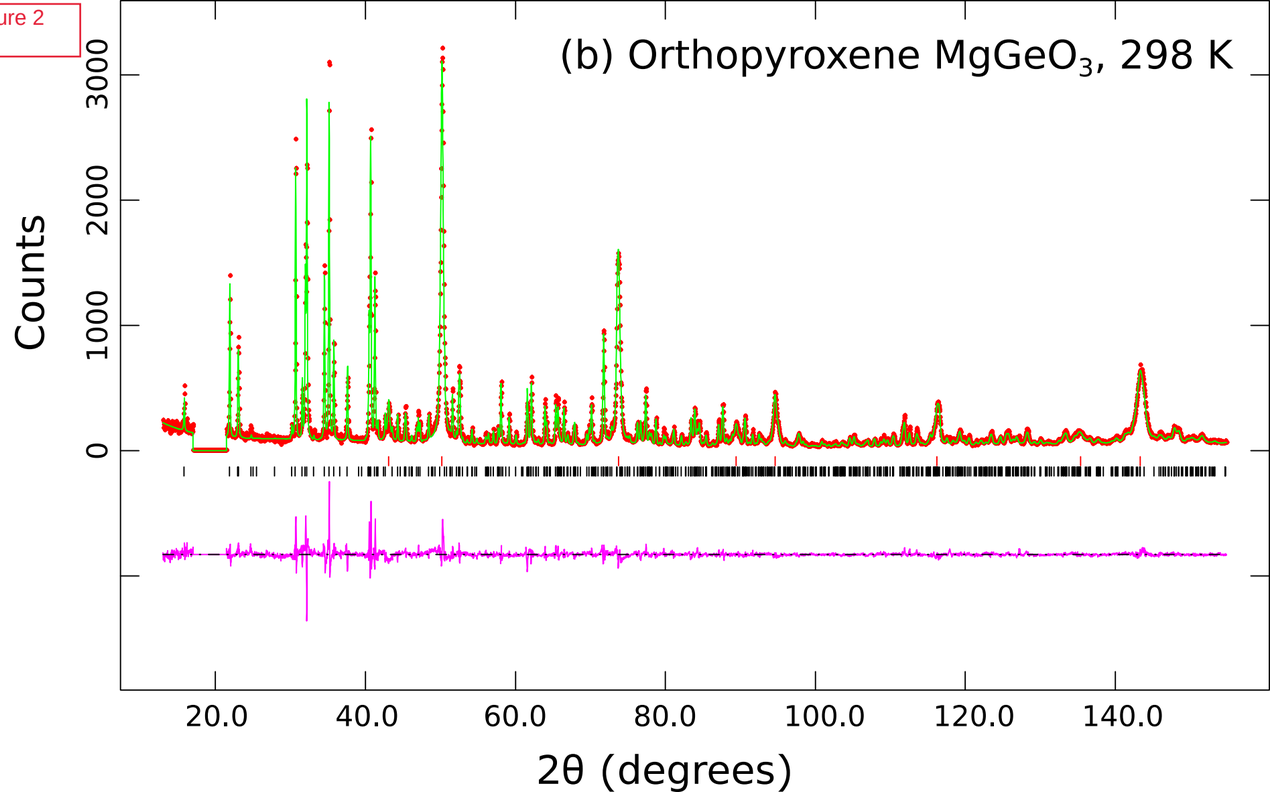
(b) Orthopyroxene MgGeO3, 298 K
Counts
0
1000
2000
3000
20.0
40.0
60.0
80.0
100.0
120.0
140.0
2θ (degrees)

Figure 3

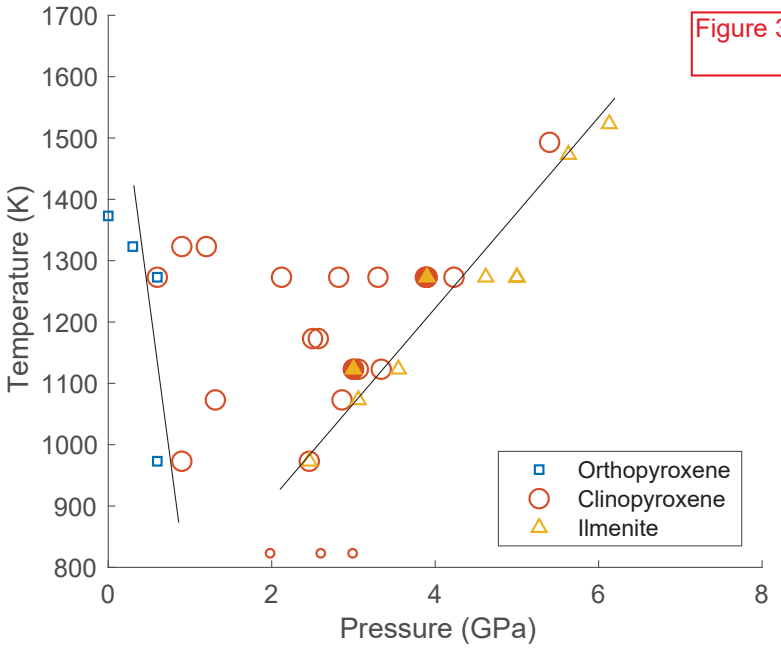
Temperature (K)
Pressure (GPa)
Orthopyroxene
Clinopyroxene
Ilmenite

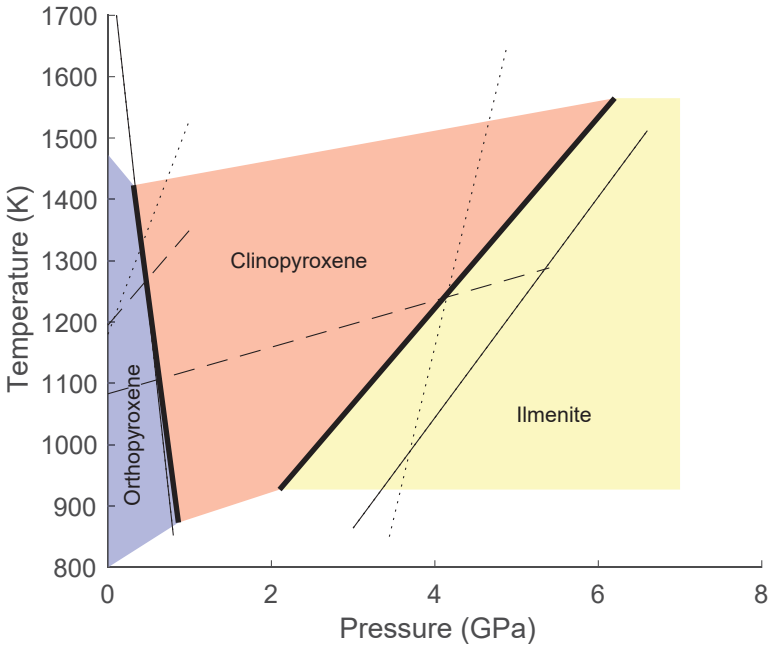
Temperature (K)
Pressure (GPa)
Clinopyroxene
Orthopyroxene
Ilmenite

Figure 4

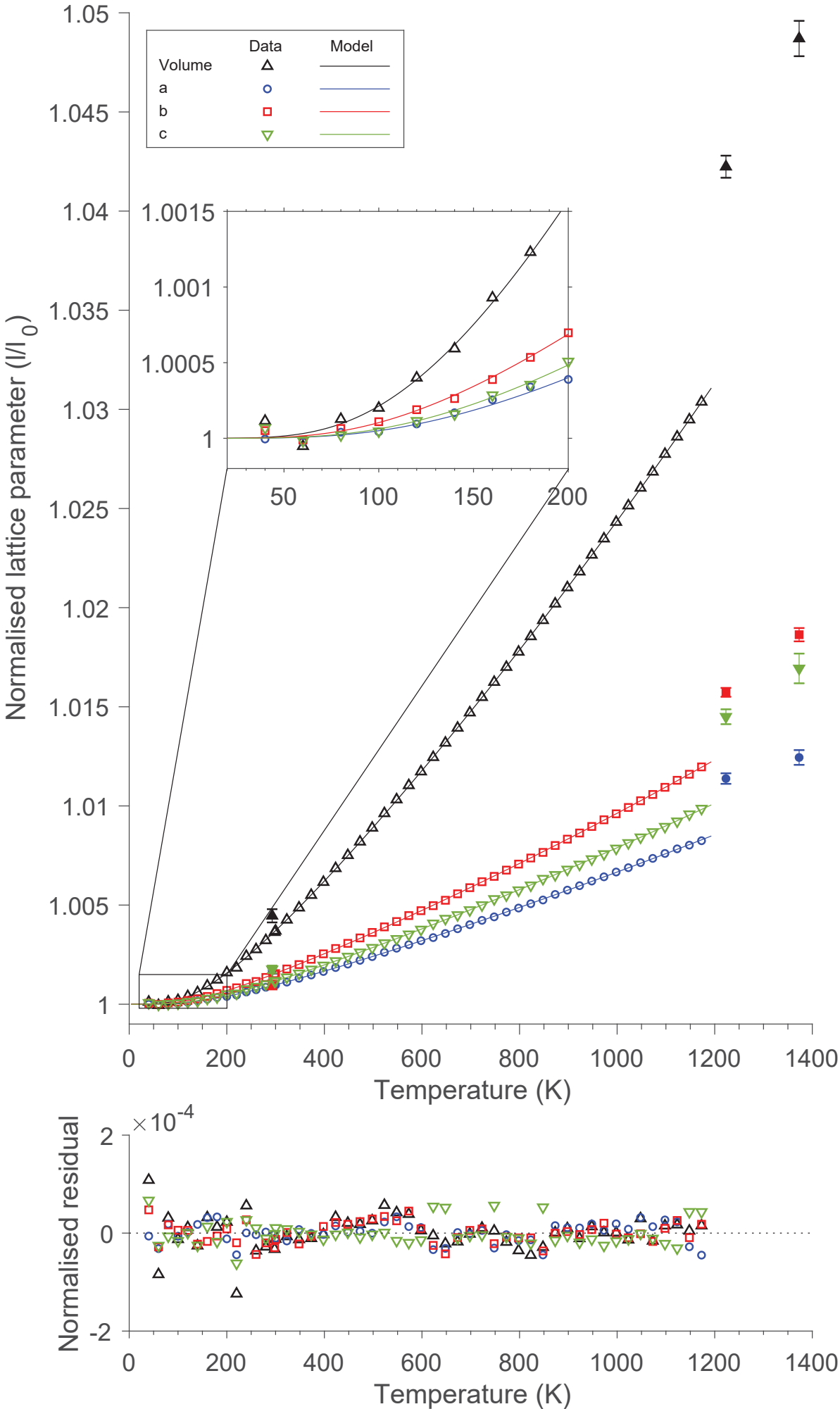
Data
Model
Volume
a
b
c
Normalised lattice parameter (l/l0)
Temperature (K)
Normalised residual
×10-4

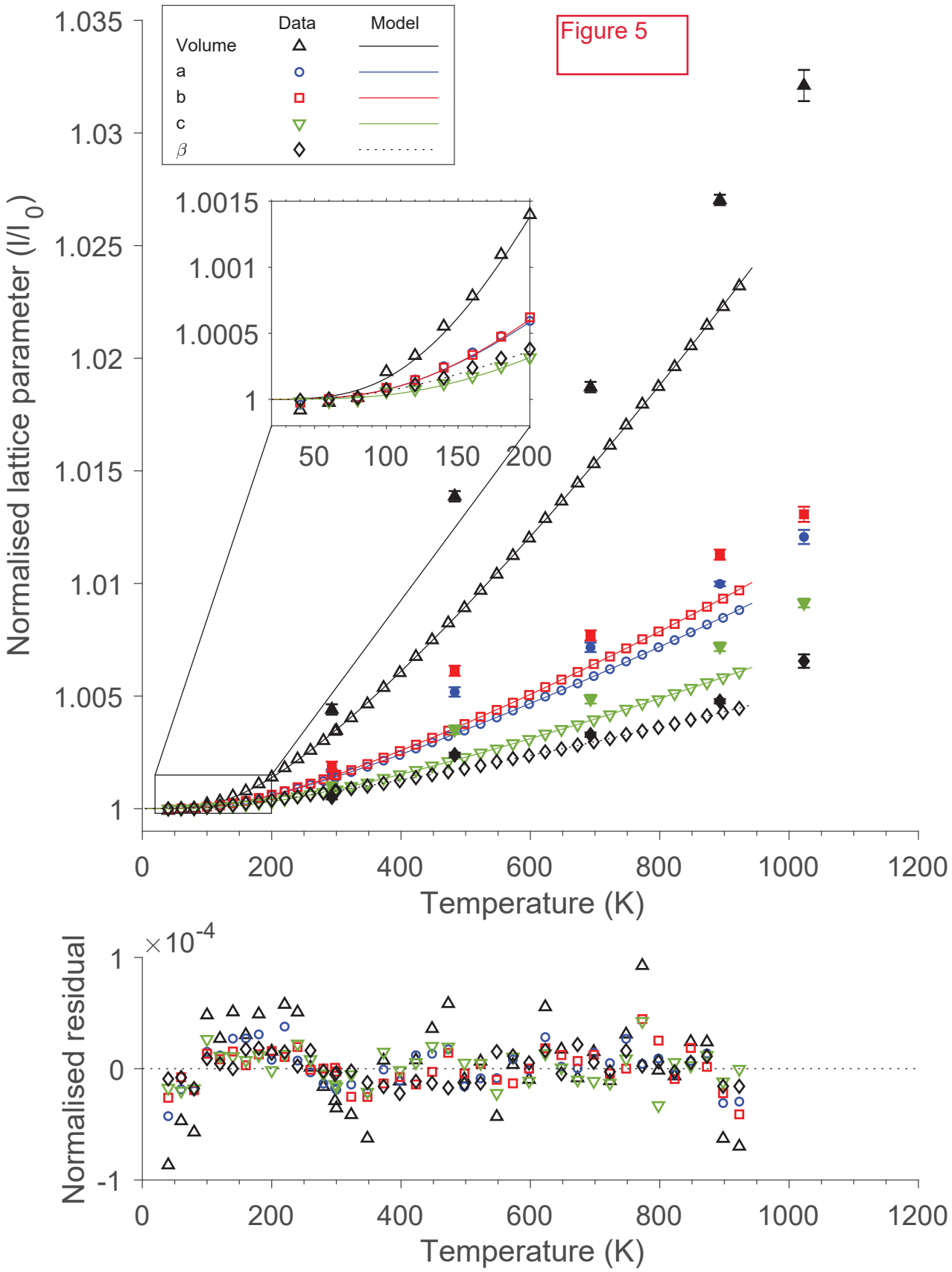
Figure 5
Data
Model
Volume
a
b
c
β
Normalised lattice parameter (l/l0)
Temperature (K)
Normalised residual
×10-4

Figure 6

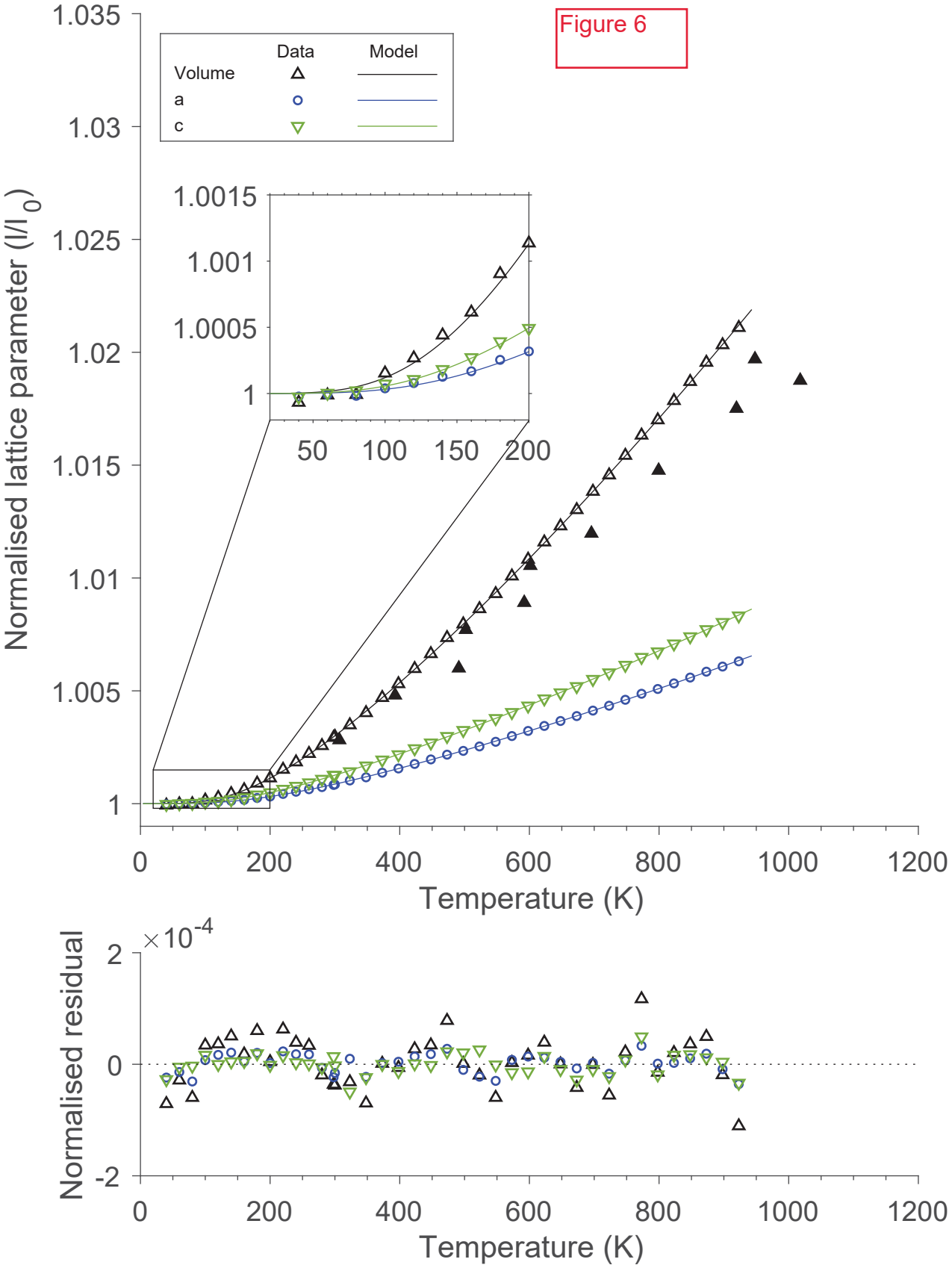
Data
Model
Volume
a
c
Normalised lattice parameter (l/l0)
1.035
1.03
1.025
1.02
1.015
1.01
1.005
1
1.0015
1.001
1.0005
1
50
100
150
200
0
200
400
600
800
1000
1200
Temperature (K)
×10-4
2
0
-2
Normalised residual
0
200
400
600
800
1000
1200
Temperature (K)

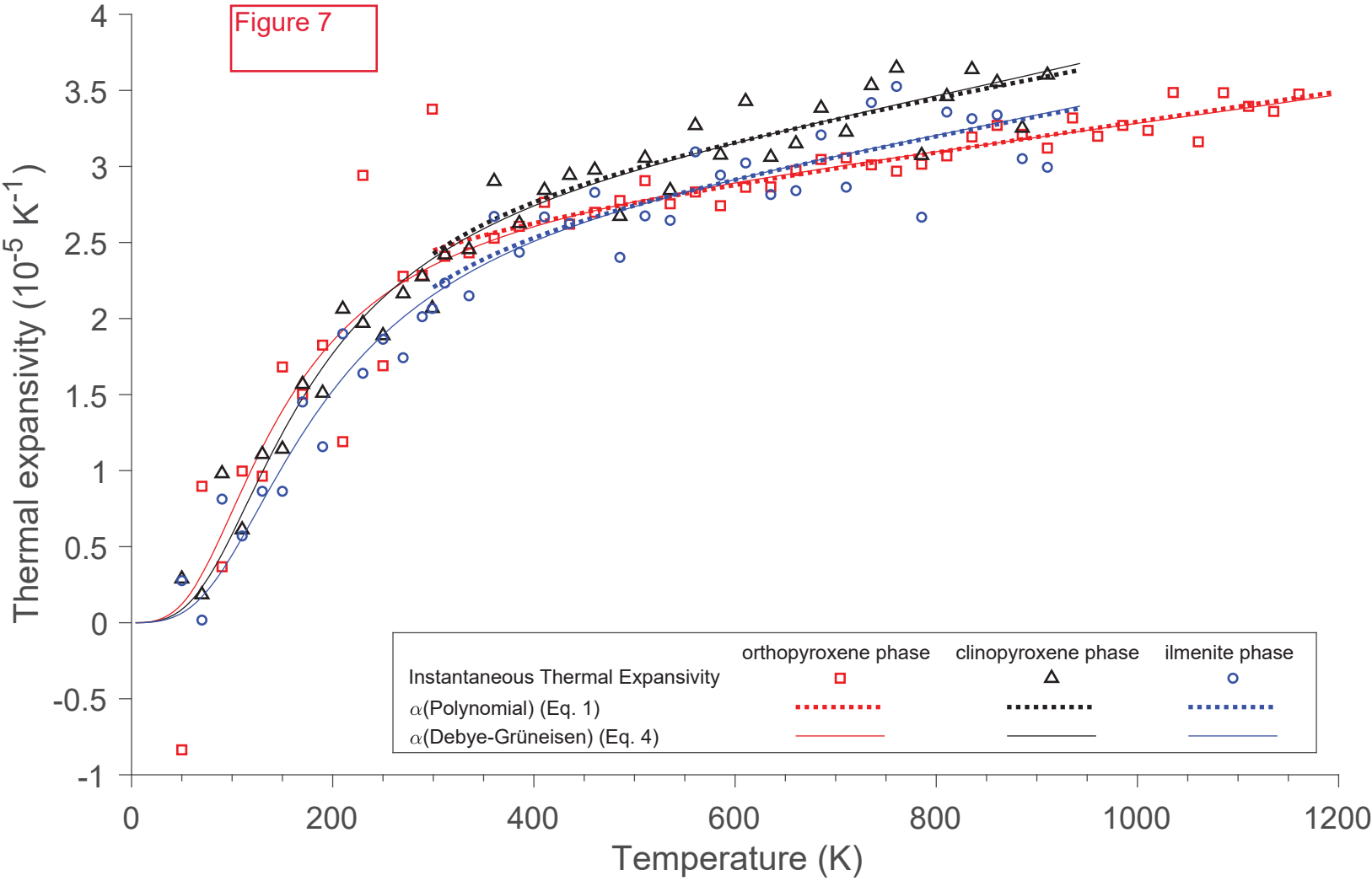
Figure 7
Thermal expansivity (10^{-5} K^{-1})
Temperature (K)
4
3.5
3
2.5
2
1.5
1
0.5
0
-0.5
-1
0
200
400
600
800
1000
1200
orthopyroxene phase
clinopyroxene phase
ilmenite phase
Instantaneous Thermal Expansivity
α(Polynomial) (Eq. 1)
α(Debye-Grüneisen) (Eq. 4)

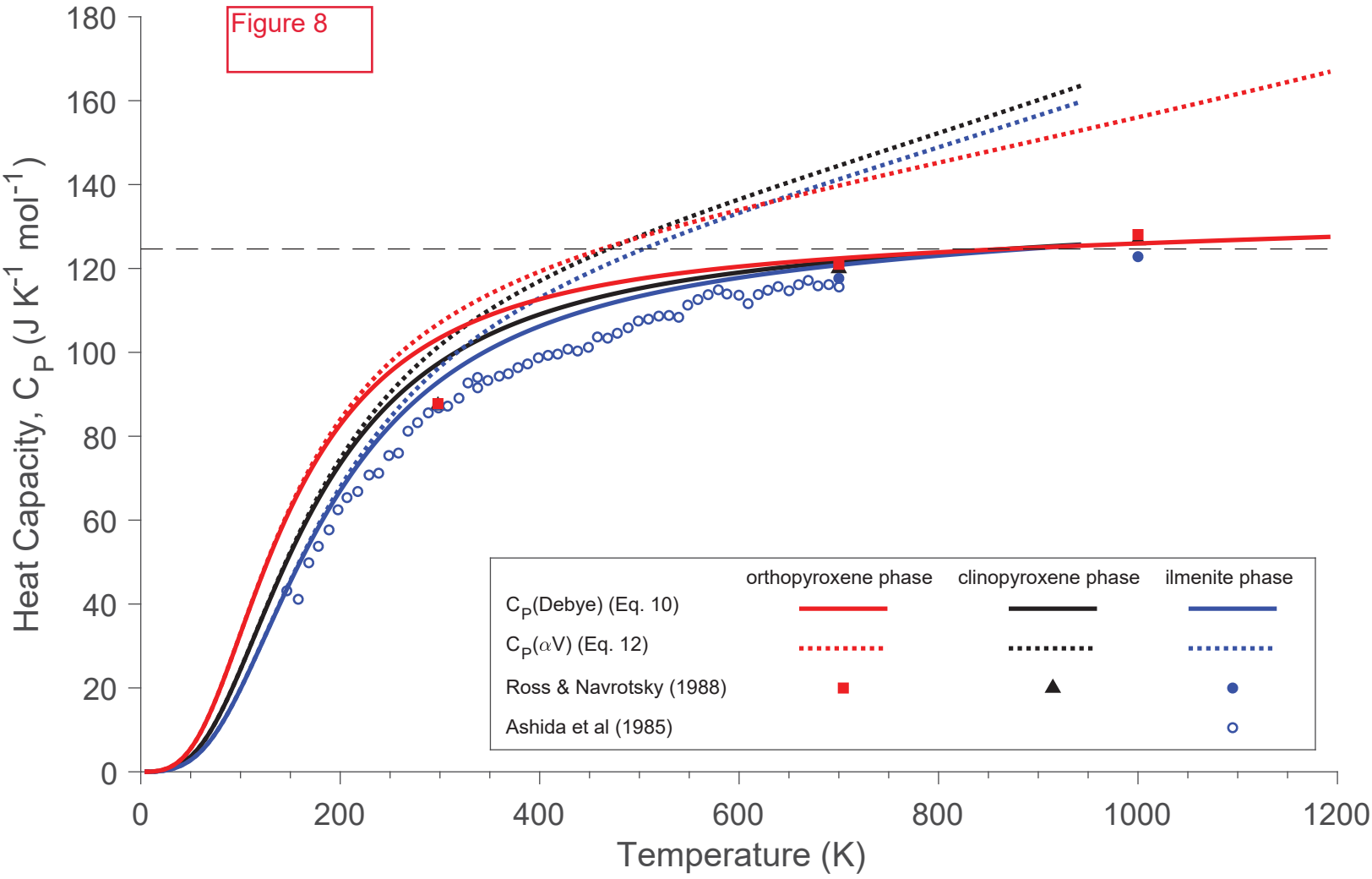
Figure 8
Heat Capacity, C_P (J K^{-1} mol^{-1})
Temperature (K)
0
20
40
60
80
100
120
140
160
180
0
200
400
600
800
1000
1200
orthopyroxene phase
clinopyroxene phase
ilmenite phase
C_P(Debye) (Eq. 10)
$C_P(\alpha V)$ (Eq. 12)
Ross & Navrotsky (1988)
Ashida et al (1985)

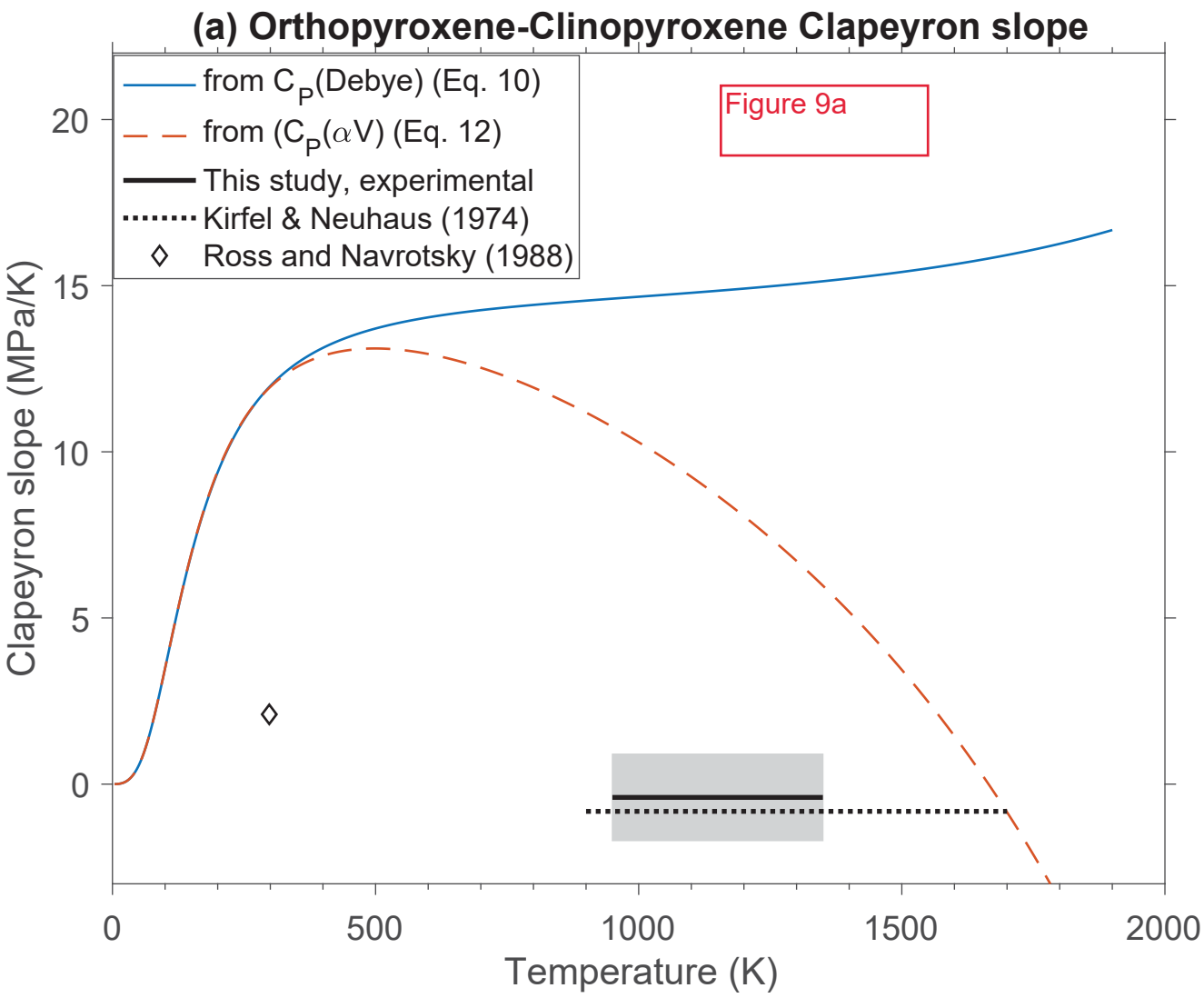
(a) Orthopyroxene-Clinopyroxene Clapeyron slope
from C_P(Debye) (Eq. 10)
from (C_P(αV) (Eq. 12)
This study, experimental
Kirfel & Neuhaus (1974)
Ross and Navrotsky (1988)
Figure 9a
Clapeyron slope (MPa/K)
Temperature (K)
0
5
10
15
20
0
500
1000
1500
2000

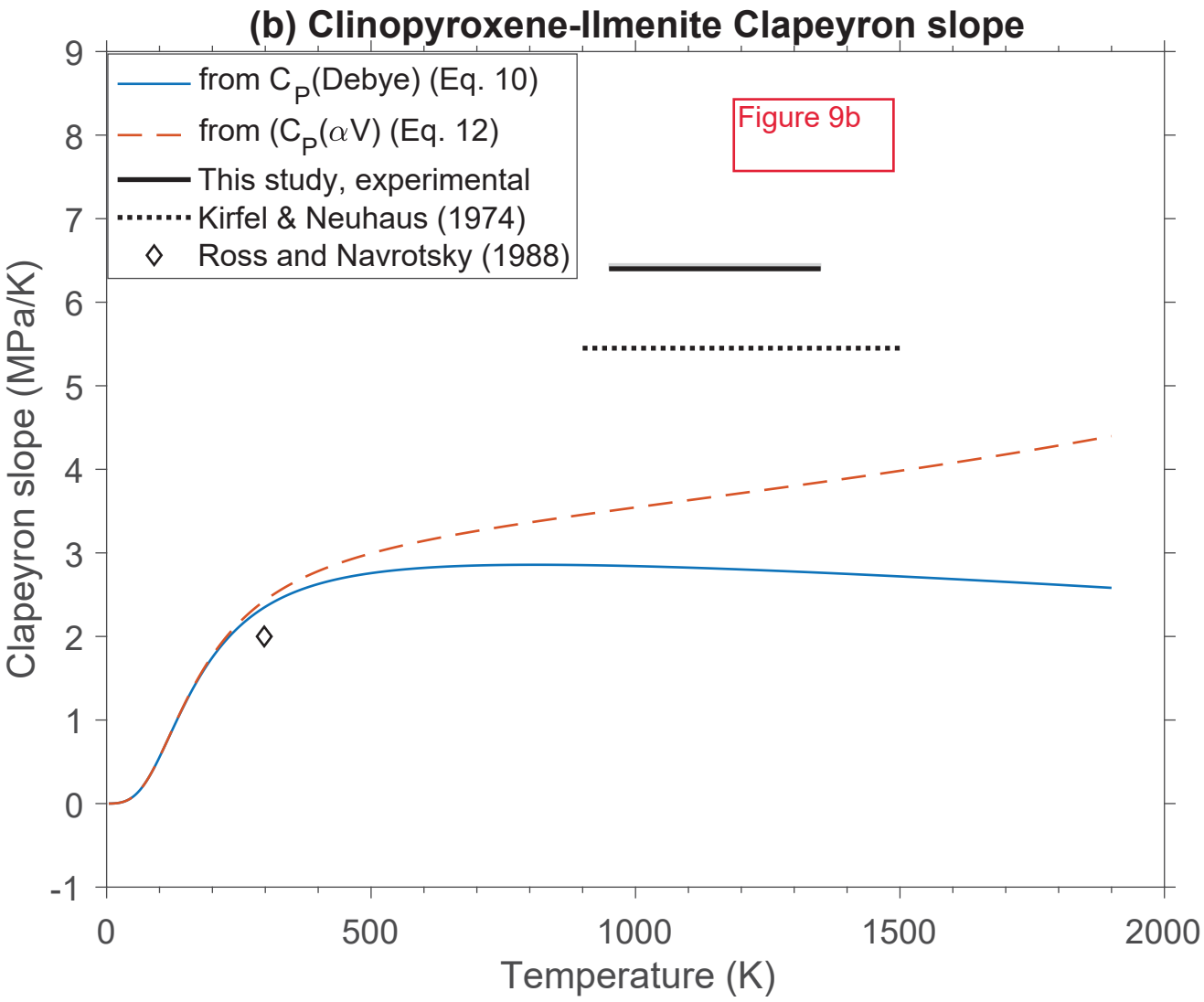
(b) Clinopyroxene-Ilmenite Clapeyron slope
from C_P(Debye) (Eq. 10)
from (C_P(αV) (Eq. 12)
This study, experimental
Kirfel & Neuhaus (1974)
Ross and Navrotsky (1988)
Figure 9b
Clapeyron slope (MPa/K)
Temperature (K)
9
8
7
6
5
4
3
2
1
0
-1
0
500
1000
1500
2000